Transverse finger bars at the Gold Coast

MPOC Master thesis

Anneke ten Doeschate

Supervised by:
Prof. dr. Huib E. de Swart
Dr. Gerben Ruessink
Dr. Cesca Ribas

Institute for Marine and Atmospheric research Utrecht (IMAU)
Utrecht, the Netherlands
Universitat Politècnica de Catalunya (UPC)
Barcelona, Spain

August 10, 2012

Abstract

Sandy beaches worldwide often display pronounced morphological features, such as crescentic bars, rip channels and beach cusps. Sometimes also a less well known pattern of transverse finger bars develops. These bars are relatively small, attached to the inner bar or the shoreline, and have in general an oblique orientation. Four years of time-exposure images permit to study the occurrence of transverse finger bars in the surf zone of a beach on the Gold Coast, East Australia. Transverse finger bars are thus observed to occur here on 24% of the study period. The finger bars occur in patches of 3 to 15 bars, with an average transverse finger bar event duration of 5 days. The presence of bars is related to intermediate energy wave conditions. When the offshore wave height is higher that 1.2m., transverse finger bars are never observed. In the majority of the cases, the crests of the transverse finger bars point against the direction of the incoming waves: up-current oriented bars. The hypothesis that, apart from the wave conditions, also the overall morphology of the nearshore zone is of influence to transverse finger bar development, is tested by looking to the shape of the shore parallel bars at the time of transverse finger bar occurrence. Is is shown that finger bar occurrence is often coinciding with a state of the shore parallel bars that reflects low to intermediate energy conditions.
A morphodynamic model has as well been applied to investigate the Gold Coast transverse finger bars. This model describes self-organization processes in the nearshore zone: the feedback between waves, breakers, depth-averaged currents and bed evolution. The model proved capable of describing the initial growth of up-current transverse finger bars with characteristics corresponding well to the observations. The model has been used to study the mechanism of transverse finger bar growth. It explains why only waves with a minimal offshore angle of 20° with respect to the shore normal, and an intermediate height promote transverse finger bar growth. The longshore current is found to be the main factor controlling transverse finger bar formation, although also the effect of the turbulent sediment resuspension by the rollers formed on wave breaking plays a role.

Preface

With this thesis work I finally finish my studies at the IMAU institute. It has been a sometimes tough, but very interesting three years of study. I would like to thank my parents for always having supported me. I would like to thank Huib for the inspiration he gave in his courses and how he almost to the end of the project could inspire me to work on. To Gerben the honours to take over on this in the final weeks. The group of Albert Falqués, Cesca, Daniel, I would like to thank for receiving me at their office in the sunny Barcelona for five months, and to let me take part in their scientific and social activities. I hope your small group may endure! And some final thanks to Ändu, for making the time in Barcelona even more interesting.

Contents

1 Introduction

In various parts of the world coastal lands are bordered by elongated sandy beaches e.g. the Dutch North Sea coast, the coast of Aquitaine (France) bordering the Atlantic, the Mediterranean beaches South of Barcelona, wide beaches in Namibia, and both the East and West side of Australia. The various beaches are not all the same, but vary under different wave conditions and the environmental setting, which both again vary spatially and temporally.

Wright *et al.* (1979) and Wright & Short (1984) defined a classification of beaches into different states, dependent on the antecedent wave conditions, the local environmental shape and the sediment characteristics.

In the nearshore zone of these sandy beaches, one often can observe that the approaching waves deform and eventually break, with more or less heavy plunging and foam production. In this breaker zone, the surf zone, waves induce currents and turbulent motions which influence the sea bed morphology. There is a strong feedback between these hydrodynamics and the evolution of the sandy bed. When taking a closer look, one may see that the sea bed of the beach face, intertidal and sub-tidal zone is not smooth, but has a specific morphology with a spatial and temporal variation. Especially during relatively fair weather conditions, the morphodynamic result is a certain rhythmic topography: typical bed forms in the surf zone and the beach face, that occur repeatedly in alongshore direction. Examples of rhythmic topography that are commonly observed in the nearshore of sandy beaches are crescentic and transverse sand bars and beach cusps, illustrated in figure 1.1.

Figure 1.1: Examples of rhythmic bed forms associated to sandy beaches. Left the beach of Truc Vert (French Atlantic), where preferential breaking on crescentic bars in the surf zone can be observed, with rip channels in between. Right image shows Hammer Head beach (SW Australia) with beach cusps developing on the shore line

The topic of this research project is another specific type of rhythmic topography: transverse finger bars. Transverse finger bars are elongated sand bars in the sub-tidal part of the surf zone of sandy beaches. The bars have a cross-shore length of about 50 meter, and are attached to the beach line or a shore parallel sand bar. The crests extend in seaward direction with a certain obliqueness with respect to the shore normal. Finger bars occur in patches of several bars next to each other with a regular spacing.
Transverse finger bars have been observed and described in literature by Konicki & Holman (2000), for a beach near Duck, North Carolina (USA). They report bars that extend seaward both from the shoreline as from a shore-parallel sand bar. The average inter-bar spacing of the first, the 'trough-bars' was 79 meters. The crest lines of the fingerbars in general were seen to point against the direction of the main longshore current; the bars had an up-current orientation. At times the bars were seen to move in the direction of the longshore current with migration rates up to 40 m/day.

Ribas & Kroon (2007) did an extensive analysis of transverse finger bars observed at Noordwijk beach, the Netherlands. The here described finger bar characteristics comprise an average spacing of 39 meters, also with in general an up-current orientation. It is remarked that fingerbars are only present when the distance to the next shore parallel bar, the trough area, is wide enough. Both the beaches of Duck and Noordwijk are part of an open coast, subject to an intermediate to higher energy wave climate. It is during the calmer intermediate wave conditions that fingerbars have been observed at these beaches.

A useful method to study the nearshore morphology for both scientific and coastal management reasons, is by means of an ARGUS videoimaging system. The system consists of four to five camera's installed on a higher place near to the beach, which together provide a continuous 180°-view of the coastline during daytime hours. Both the observations of transverse finger bars at Duck and at Noordwijk were done by means of an ARGUS video images. Figure 1.2 shows an example of the 180°-view the ARGUS system gives over the nearshore zone.

Figure 1.2: Example of a time-exposure image taken on the 4th of August 1999 by the ARGUS system at the Gold Coast, Australia

But, why is it so interesting to study transverse fingerbars? Comparing the spatial scale of transverse finger bars to other rhythmic patterns in the surf zone, they are smaller than crescentic bars and rip current systems. The deviation of the flow around transverse finger bars is not as strong that it has an important effect on coastal evolution, neither on coastal safety.

However, the transverse finger bars are the visible result of the physical mechanisms that dominate the evolution of the morphology of the nearshore zone. Studying the formation of fingerbars will improve understanding of the governing mechanisms in this zone. To gain a deeper understanding of their formation it is essential to further compare model results to observational data.

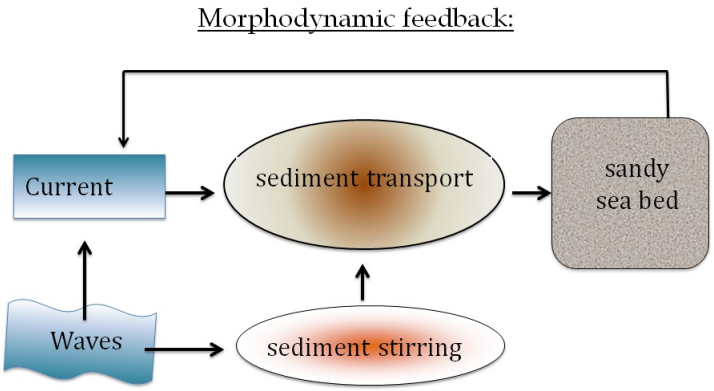

Figure 1.3: The concept of morphodynamic self organization: Waves and currents will transport sediments, that change the sea bed locally. An initially small morphologic feature will feed back on the local hydrodynamics. If the feedback between bed perturbation and flow is positive, the bed perturbation may develop furthe.

How can the development of transverse finger bars during intermediate energy wave conditions than be explained? Niederoda & Tanner (1970) already described the formation of large transverse bars, stating that their geometry made incoming waves refract in a way that wave energy is focussed over de bar crest, thus promoting further bar growth. Konicki & Holman (2000) tested whether transverse bars could be explained from a longshore current instability mechanism, to conclude that on an open coast there is no direct relation between bar presence and currents only, but that wave effects should be taken into account too.

Then Ribas & Kroon (2007) suggested that transverse finger bar formation is the result of morhodynamic self-organization mechanisms in the surf zone. The concept of morphodynamic self organization is based on stability analysis: a small developing sea bed feature may change the flow and sediment transport in a way that promotes further growth of that feature. A positive feedback between the bed, waves and currents, and sediment transport is thus established. Figure 1.3 summarizes the concept of morphodynamic self organization schematically.

The mechanism that would result a positive feedback regarding transverse finger bar growth, consists of an offshore deflection of the longshore current over the crest of the finger bar, compensated by a shoreward flow through the deeper parts between the bars. (Ribas *et al.* (2003)). This flow deflection, together with a depth integrated sediment concentration that decreases in seaward direction, promotes growth of finger bars with an up-current orientation. To force the longshore current, the incoming waves should be oblique.

Ribas *et al.* (2011b), Ribas *et al.* (2011a) used an existing morphodynamic model, MORFO60 (Calvete *et al.* (2005), that describes the feedback between waves, depth-averaged currents, free surface evolution and bed evolution. The model is based on a linear stability analysis, They extended this model with roller dynamics, the roller being the turbulent, foamy front of a wave when it is breaking in the surf zone. The model proved capable of predicting the longshore current, and the development of up-current oriented finger bars in good agreement with observations from Noordwijk beach, and Duck beach as well. The rollers are indispensable in this result, since their turbulent 'bores' lead to a sediment resuspension, such that the depth integrated sediment concentration decreases seaward across the inner surf zone. Ribas *et al.* (2012) further explored the physical mechanism of the roller dynamics with the updated model,

MORFO62. It is found that the rollers have a dual effect, both promoting and damping the development of transverse finger bars. The angle of wave incidence determines for a large part which of the two mechanisms is dominant. For oblique waves, the effect of the rollers promotes an offshore deflection of the current over the fingerbars, whilst also this current itself is stronger.

Until now the model has been validated for only two beaches. Both Noordwijk and Duck beaches are part of an open coast, with a relatively gentle slope. Although not further reported in literature, it may very well be that transverse finger bars are occurring on other beaches too. If so, will the self-organization model again be able to explain and predict the formation of fingerbars there?

In this project therefore another beach is studied: Surfer's Paradise beach, located on the Gold Coast, state of Queensland, Australia. The Gold Coast is an extended, straight coast bordering the Southern Ocean, with wide sandy beaches. The study site differs from Duck in the first place because the bed slope of the nearshore zone is twice as steep, Noordwijk having an even more gentle offshore slope. The average wave climate is comparable, although at the Gold Coast periods of severe storms are more frequent. Another difference between the Gold Coast versus Duck / Noordwijk, is that in the surfzone of the Gold Coast in general two alongshore bars are present, instead of only one.

Surfer's Paradise beach is monitored for coastal zone management-purposes by an ARGUS video system since 1999. However, next to studying the effect of human interventions on the beach, like beach nourishments, the video images have also been used to study the morphology of the surf zone for pure research purposes. Ruessink *et al.* (2009); Price & Ruessink (2011) studied the variation of the alongshore bars in the nearshore zone of Surfer's Paradise beach, by means of the ARGUS- images. During these studies also transverse finger bars have been seen. These are adressed here.

The research questions about the Gold Coast transverse finger bars are the following:

- How often do transverse finger bars occur in the surf zone of Surfer's Paradise beach? What are their characteristics?
  Does the size, wavelength and orientation of the finger bars correspond to those observed at Duck and/or Noordwijk?

- Under what conditions do the finger bars develop? Is their development related to the offshore wave conditions? What is the role of the total surf zone morphology?
  The shore parallel bars in the nearshore zone can be changing a lot over time, as a result of variable energy conditions. It may well be that transverse finger bar presence is promoted by a typical configuration of the alongshore bars

- Can the model MORFO62 be used to predict the growth of transverse finger bars at the Gold Coast? Do predicted finger bar characteristics correspond to the observations?

- What does the model tell about the conditions under which finger bar growth occurs? Is this in correspondence to the observations as well?
  Do the results prove that transverse finger bars result a self-organization process forced by the longshore current and the dynamics of the turbulent rollers?

To address these questions, four years of ARGUS time-exposure images have been studied, to locate and describe the occurrence and shape of the transverse finger bars at Surfer's Paradise beach. Coupling this to regional information about the properties of the incoming waves will give an impression about the environmental conditions required for finger bar growth.

Typical wave conditions will serve as a default input to the morphodynamic model. If the default output indeed predicts that transverse finger bars will grow under the specified conditions, the characteristics of modelled and observed bars can be compared. Sensitivity analyses to the wave conditions that provide the limits of the transverse finger bar growth hopefully compare to the limits deduced from the observations.

The report starts with a chapter in which I go further into the backgrounds of the nearshore zone: the morphology and hydrodynamic processes which occur there. Here also the mechanisms thought to be involved in transverse finger bar growth are presented. In chapter 3 the reader is introduced to the study site, the observational data present and the setup of the morphodynamic model. The results are presented in chapter 4, the chapter being split up in a section on the analysis of the ARGUS images of Surfer's Paradise beach, and a section presenting the model results for the default case and the results from an extensive sensitivity analysis. Chapter 5 forms a discussion that critically reflects on the main results, followed by a conclusion in chapter 6.

2 Background

In the introduction many terms were mentioned without clearly explaining them. For a better understanding of the project, in this chapter some general aspects of the study domain, the nearshore zone, and it's morphology are presented. Next to that the hydrodynamic processes that are possibly involved in the formation and behaviour of transverse finger bars are described.

2.1 The nearshore zone

Transverse finger bars are a morphological phenomena observed to extend 50 to 70 meters seaward from the beach, in depths of 1 to 2 meter. This means that they are a phenomena of the upper part of the 'shoreface'. The exact definition of the shoreface is a bit ambiguous, but here the definitions and classification given in Short (1999) is followed: the shoreface is the part of the littoral zone from the limit of wave run-up on the beach, extending seaward until the depth limit of gravity waves to have an influence on the sediment at the sea bed; further seaward, in deeper water, the sediment will not be stirred or transported by the instantaneous wave field any more. This offshore limit is therefore also called the 'wave base'. However it is hard to locate exactly, since the location of the closure depth varies when regarding different time scales.
The shoreface is a geomorphic feature, dividable into smaller zones characterised by different processes. Although transverse finger bars are found close to the beach, the waves that are said to be an important factor in the development of the bars, travel through all these different zones and interact with them. It is therefore useful to take a closer look on the complete region.

An illustration of the different zones is shown in figure 2.1. A first division is made between the 'lower' and 'upper' shoreface. The upper shoreface is defined as the region in which erosion and accretion result in measurable changes of the seabed profile in a typical year. It is continuously in a state of dynamic equilibrium, subject to instantaneous changes of its boundary conditions, the properties of the incoming waves. A true equilibrium is seldom reached, due to the variability of those waves. The lower shoreface extends from the upper-shoreface closure depth offshore to the shoreface limit. Only storm-event coupled changes and other low frequency variability will invoke measurable changes of the lower shoreface. The gradual un-deepening of the water depth of the shoreface induces wave shoaling. Within the upper shoreface the shoaling region and the surf zone are defined, the surf zone being the part of the nearshore where incident waves break and breaking-induced processes dominate the fluid motion and sediment transport processes. It is this last domain on which this study is focussed, since it is there that the transverse finger bars can be observed.

To be exact, as shown in figure 2.2, the surf zone may be divided into different regions again, according to the different stages of wave transformation. In nature one will always see an irregular wave field, thus breaking will not occur at one specific location. The larger waves of the wave distribution will break previously, in the 'outer surf zone', whilst the majority of the

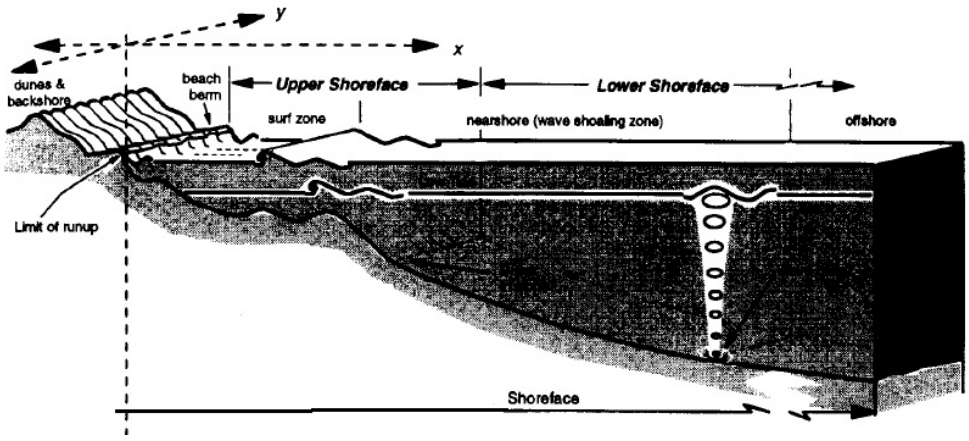

Figure 2.1: A schematic drawing of the shoreface and the location of the different zones defined within it. Picture taken from Short (1999).

waves break in the 'inner surf zone'. Underlying topography near the shore, like longshore and transverse sandbars, provoke breaking of waves too. The zone where the waves run up and back down the beach face is called the 'swash zone', or 'run-up' region. The location of this zone is variable, changing with the strength of the waves and eventually also the tidal cycle.

2.2 Hydrodynamic processes

Waves

Studying shoreface evolution implies the analysis of changes in the equilibrium between the sea bed profile, the beach form and the water motion. The hydrodynamics of the shoreface are governed by wave motion and currents. To start with the waves, these originate from wind and swell in offshore regions. Wind is a turbulent forcing, resulting an irregular wave field regarding frequency, height and propagation direction. A generally accepted way to describe this field is

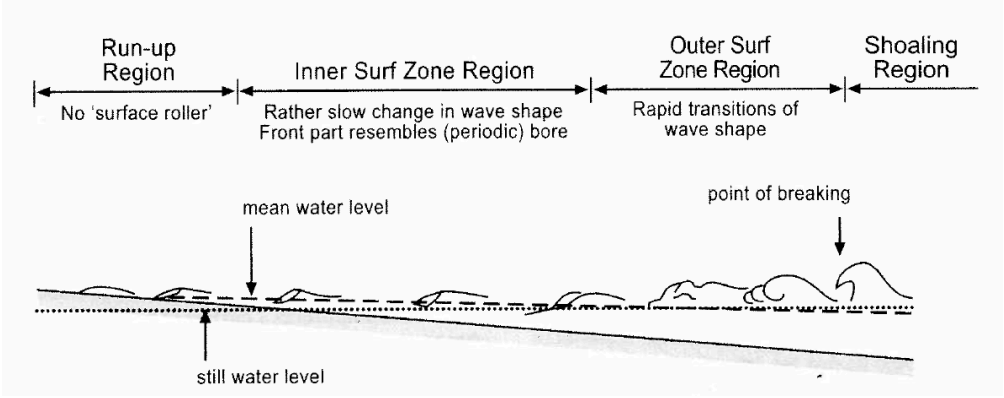

Figure 2.2: Wave transformation in the surf zone. From Short (1999).

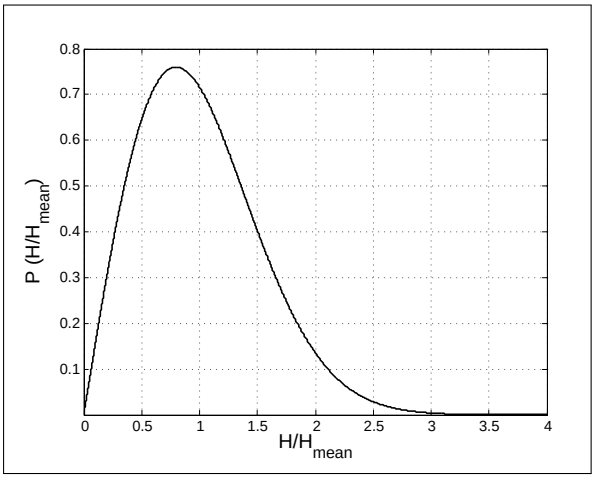

Figure 2.3: Rayleigh distribution of the normalised wave height (H/H_{mean}). From Short (1999).

the Rayleigh distribution, a probability distribution of wave height with an asymmetric shape (see figure 2.3). The root mean square wave height, H_{rms} is based on this distribution. It is an often used parameter to represent the energy of the wave field:

$$H_{rms} = \sqrt{\frac{\sum H_i^2}{N}}. \tag{2.1}$$

An other way to describe the field of waves is a spectral analysis, where the wave energy is plotted as a function of the wave frequency. From this method the commonly used indicator T_{peak} is determined. This 'peak period' is the wave period associated with the maximum wave energy of the spectrum.

Offshore the shoaling zone the waves can be considered linear short waves, under the assumptions that the wave amplitude is small with respect to both the wave length and the total water depth, and that this total depth is varying on a spatial scale much larger than the average wave length. Linear waves can be described by:

$$\sigma^2 = g\kappa \tanh(\kappa D). \tag{2.2}$$

$$\phi = \frac{\sigma}{\kappa} a \frac{\cosh[\kappa(z+D)]}{\sinh(\kappa D)} \sin(\vec{\kappa}\cdot\vec{x} - \sigma t). \tag{2.3}$$

$$\zeta = a\cos(\vec{\kappa}\cdot\vec{x} - \sigma t). \tag{2.4}$$

σ : frequency [Hz], $\vec{\kappa}$: wave vector, D : waterdepth[m], g : gravity acceleration[ms^{-1}], t : time[s], ϕ : velocity potential, $\vec{x}$: position in the horizontal plane (with components x and y), z : vertical postion.

The wave vector $\vec{\kappa}$ has length κ and points in the direction of wave propagation. The propagation speed of the wave, the ' phase velocity', is the ratio of the frequency over κ:

$$c = \frac{\sigma}{\kappa}. \tag{2.5}$$

κ describes the number of waves per unit of distance, so it is the reciprocal of the wave length; $\lambda = 2\pi/\kappa$. The wave vector can be decomposed in two components along the x- and y-axis: $k = \kappa \cos\theta$ and $l = \kappa \sin\theta$ respectively.

In the above equation (2.2) is the dispersion relation, the relation between wave frequency, phase velocity and wavelength. The velocity field of the sea water is irrotational, current velocities are determined as the gradient of the velocity potential of the flow in equation (2.3). Equation (2.4) describes the free surface elevation due to the wave motion. When a wave propagates through a deep water mass, the water particles locally describe an orbital motion. However these orbits are not fully closed, so that waves cause a net mass flux of water in the direction of wave propagation. This flux is known as 'Stokes' drift. The movement of the water, the orbital motion, is highest at the surface, and reduces towards the bottom. When the flow enters a shallower zone, the particle orbits will flatten.

The energy density of the total wave field is described by

$$E = \frac{1}{8}\rho g H_{rms}^2. \tag{2.6}$$

Energy is transported with the group velocity:

$$c_g = \frac{\partial \sigma}{\partial \kappa}. \tag{2.7}$$

In the shoreface region the water depth gradually decreases shoreward. Here the energy of the waves will become compressed, the energy density increases. According to equation (2.6) this results in a gradual increase of the wave height too. The surface profile of the waves will thereby deform, become more and more different from the original sinusoidal profile: the waves steepen and shorten, which under the assumption that their frequency does not change, goes together with a decrease of the phase velocity. The whole of shortening and steepening of the waves in the nearshore zone is called 'wave shoaling'. Steepening cannot go on forever, the wave form will finally become unstable and breaking will occur. Maximum wave steepness can be described with the breaker index γ_b:

$$\gamma_b = \frac{H}{D}. \tag{2.8}$$

D: local waterdepth $[m]$ With the use of equation (2.8) the location of breaking of any random wave with wave height H can be determined, if the depth profile of the upper shoreface is known. Three different types of breaking can be discerned (Svendsen (2006)): spilling breaker, plunging breakers and surging breakers. In a spilling breaker the whole front side of the wave crest is made up of foam, whilst propagating towards the shore. This water in turbulent motion is called a roller, or a turbulent bore. A plunging breaker is a wave that on steepening becomes very skew. The front may be almost vertical after which the crest shoots forward and plunges down, hitting the trough in front of it. On this moment turbulence will be produced and the broken waves propagates further in a roller like the spilling breaker. Finally in a surging breaker the wave steepens, but here it is the trough of the wave front that subsequently shoots forward. This last type of breaker that does not generate much turbulent motion. The different breaker types are illustrated in figure 2.4. In spilling and plunging breakers the major part of the wave energy is turned into turbulent motion of surface rollers. It is these type of breakers that are of main concern in the formation of transverse finger bars.

Wave induced currents

Due to pressure and velocity fluctuations when waves and rollers propagate, momentum is transferred to the total water flow. These transfers are the radiation stresses, S_{xx} and S_{xy}, describing

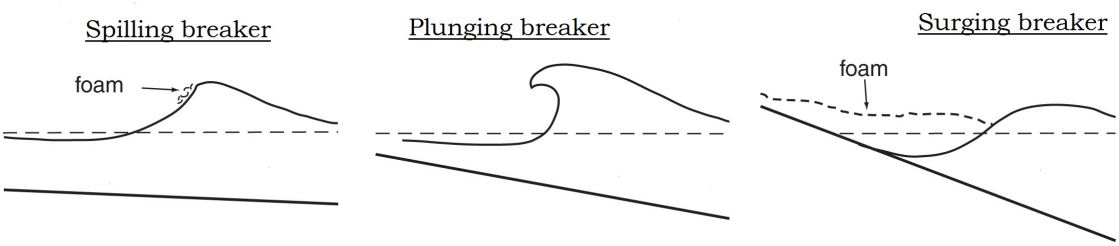

Figure 2.4: Three types of breaking waves commonly encountered in the surf zone of sandy beaches: spilling, plunging and surging waves.

the cross-shore respectively the alongshore component of the cross-shore momentum transfer from the waves to the currents. They were first introduced by Longuet-Higgins & Stewart (1964). One can make a distinction between wave radiation stresses and roller radiation stresses. Radiation stresses are a function of the wave energy density E, or the roller energy density E_{roll}, and the angle the incoming waves make with respect to the shore-normal, θ. The excess flow of momentum due to the waves, pushes the water level up at the shoreline, so that the mean water level here is higher than the average sea level a little further seaward. This is illustrated in figure 2.5. In fact the momentum balance prescribes that the gradient in the cross shore component of the radiation stresses, is mainly balanced by the wave setup, the gradient in surface elevation η.

$$\frac{\partial S_{xx}}{\partial x} \sim \frac{\partial \eta}{\partial x}. \tag{2.9}$$

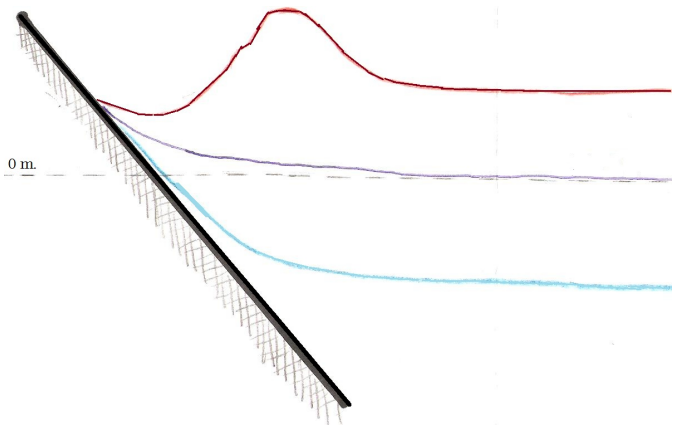

Figure 2.5: Schematical drawing to illustrate wave 'setup' at the shoreline. Red line is the average wave crest height, blue the average trough height; in purple the average of the two, representing the mean water level. Due to wave breaking the crest height reduces strongly on the break line, the trough height reduces less and at the beach line the water level is pushed up above the mean sea level (the 0m.-line).

Next to causing a setup of the waver level, the wave radiation stresses induce a typical nearshore current: the longshore current. Longshore currents are continuous shore-parallel flows that often occur in the surf zone, when incident waves are oblique. The alongshore radiation

stress S_{yx} is the component that dominantly forces this current.

$$S_{yx} = -E\big(\frac{c_g}{c}\cos\theta\sin\theta\big). \tag{2.10}$$

So the more oblique the incoming waves are, the higher the alongshore current velocity will be, velocities may exceed $1.5ms^{-1}$. The alongshore current is an important sediment transport agent (Short, 1999).

Sediment transport

Silts, sands and cobbles may be transported by water in the bedload or suspended load transport mode. Bedload transport takes place when sediment grains move whilst still being in more or less continuous contact with the sea bed: sliding, rolling or jumping. The suspended load mode is when grains are really taken up from the sea bed to be transported a lot further, along with the flow. For any transport takes place, the flow should have a minimal intensity that induces a shear stress on the sediment grains higher than the critical value. This critical value is not fixed, but depends on the type of sediment and it's grain size, but also on the slope of the sea bed. Transport under waves is dominantly forced by oscillatory motion, that causes a net sediment transport in the direction of wave propagation, knows as Stokes' drift. As mentioned earlier, an important way sediment is transported in the surf zone, is by means of the longshore current.

How does the specific morphology of the nearshore zone develop as a result of sediment transport processes? Bed forms like parallel and transverse bars and throughs are local constraints on the currents and waves, causing local flow accelerations and decelerations. A flow with a certain velocity can carry a maximum of sediment in suspension. When in a certain volume of water, more flow goes in than out, flow convergence takes place. Flow convergence implies a reduction of the flow velocity and thus of the sediment carrying capacity of the water, such that local deposition of sediment will take place. The opposite happens when flows diverge: through a certain volume more water has to pass, which results in increased flow velocities, that may erode sediments. The process of flow convergence and divergence in relation to the formation of sand bars is further illustrated in figure 2.6.

2.3 Formation of transverse finger bars

Rhythmic bed forms are developing and changing mainly under the influence of the prevailing water motion. Strong waves and currents erode sediment from the bottom, transport it elsewhere for deposition. Variability in wave and current properties results variability in this morphological evolution.

In this project the focus lies on the transverse finger bars. On the formation mechanism of up-current oriented transverse finger bars several theories exist, all explained in Ribas *et al.* (2012). They are shortly presented here. According to the concept of morphodynamic self-organization the following has to happen: on an initially growing finger bar-like perturbation the alongshore current will get deflected, and waves will deform and eventually break due to the local shallowing of the water. When the deflection is thus that an offshore flow over the bar crest is created, further growth of the bed form is promoted; this flow will experience flow divergence in offshore direction, since the total depth becomes larger. Figure 2.7 shows two hydrodynamic mechanisms that can be responsible for current deflections.

The first mechanism is based on water mass conservation, first described by Trowbridge (1995). When the longshore current flows over an elongated bar the flow velocity will increase

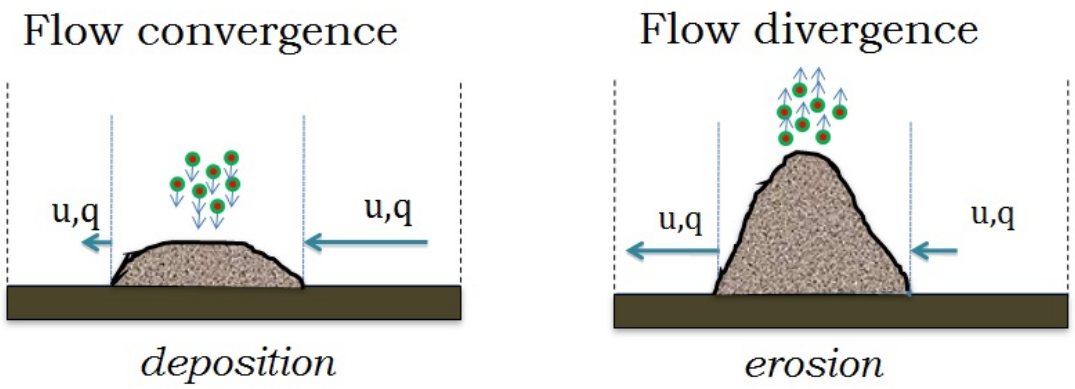

Figure 2.6: Schematical drawing to illustrate flow divergence and convergence in relation to sand bar development. Left: if a sand bar changes the flow such that flow convergence takes place over it, sediments will locally deposit. This way the sand bar will grow further. Right: when flows diverge around a certain sand bar, sediment will be eroded from it.

due to the un-deepening of the water. The cross-bar velocity component increases a lot more than the along-bar component, which results a deflection of the current in offshore direction. Besides, when water columns move from the trough onto the slope of the bar, they experience a clockwise rotation due to the friction and decreasing water depth. This effect of the 'frictional torques' was described by Zimmerman (1981).

Apart from an offshore current deflection, it is indispensable that there is a cross-shore gradient in the depth averaged sediment concentration. This gradient should be negative in seaward direction. This way the seaward deflected current will transport sediments from close to the beach along the bar crest to deeper water, where it is depositied, thus feeding the finger bar development.

Ribas *et al.* (2012) explored the effect of the turbulent surface rollers, which were included in their model. These rollers are produced on the places where the incoming waves break, e.g. over the shore parallel bar but also eventually over the finger bar crests. The turbulence forms an extra stirring, so that the sediment availability increases. But the roller radiation stresses have a dual effect on finger bar growth. If the offshore wave angle is relatively large ($\geq 30°$), the alongshore component of the radiation stresses promotes the formation of feeder currents that converge over the finger bar crests. However, the cross-shore component of the roller radiation stresses creates an onshore directed flow over the bars that dampens further bar growth. This component becomes important when the incoming waves are less oblique.

2.4 Bar state

One of the hypotheses posed in the introduction is that the presence of transverse finger bars might be related to the total morphology of the nearshore zone. This total morphology is mainly characterised by the presence of a shore parallel sand bar at a certain distance from the coastline. The location and shape of this bar, the 'bar state', is often variable over time, determined by the antecedent wave conditions, type and availability of sediment and local environmental conditions like the shelf steepness and sheltering of the beach. A commonly applied classification schedule

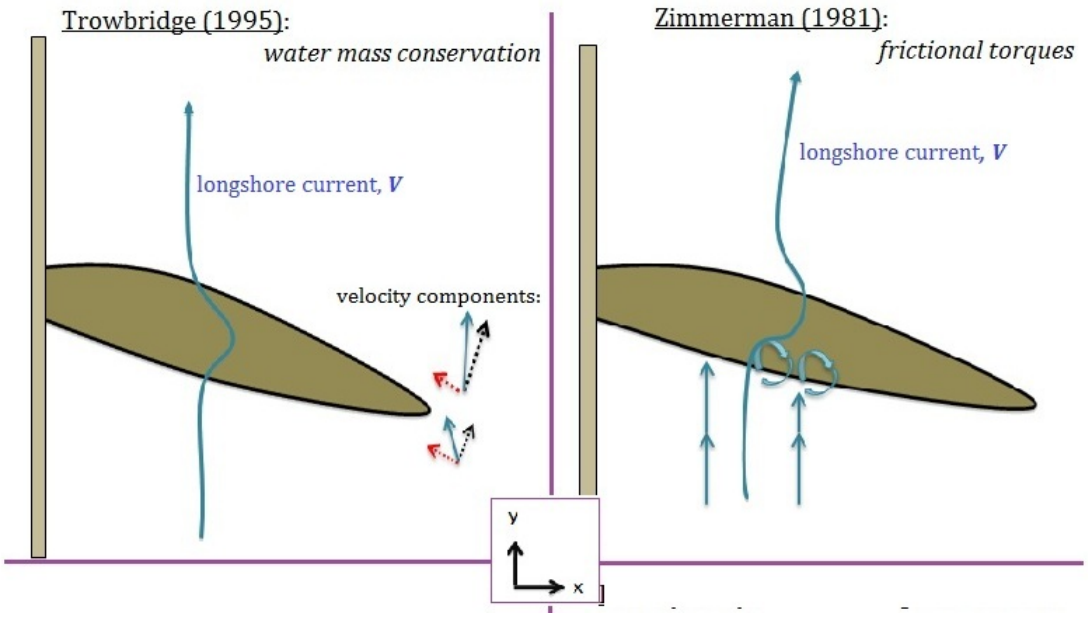

Figure 2.7: Two mechanisms to get an offshore deflection of the longshore current over an initially growing finger bar, which promotes further fingerbar growth. Upperleft: mechanism described by Trowbridge (1995), in which due to mass conservation the cross-bar component of the velocity (black dotted arrow) increases stronger than the along-bar component (dotted red arrow), resulting an offshore current deflection. Upperright: due to increased friction on the oblique bars the longshore current experiences a clockwise rotation.

for the bar state is the one developed by Wright and Short (1984). The Wright & Short bar state model defines two extreme states of the nearshore morphology, the 'dissipative' and the ' reflective' state. The dissipative state results after a persistent high-energy wave climate. It is characterized by a low-gradient beach, with a wide swash zone and a wide surf zone. The surf zone contains one or more shore parallel bars, with very few alongshore variability, which invoke wave breaking and wave energy dissipation. The reflective state results after persistent low-energy conditions, on a relatively steep beach face. There is no bar-trough system and few wave breaking takes place. The coastline is alongshore uniform, apart from eventual cusp-like features in the swash zone (Wright & Short, 1984). In between the two extreme states four intermediate states are defined. These comprise a more complex morphology, with more alongshore variability in the surf zone. Figure 2.8 gives a schematic overview of the six bar states. The first intermediate state, resembling closest to a dissipative beach, is the 'longshore bar and trough' -state (LBT). It is also characterised by a shore-parallel bar, but this one can have some curves and be crossed by rip currents. The trough is continuous and the beach line is straight, with a slightly larger beach gradient than a fully dissipative beach. The next state is the 'rhythmic bar and beach' -state (RBB). Here the parallel bar and the beach face show rhythmic curves. The bar crest has seaward protruding sections, alternated by shallower landward protruding crescentic bars. Waves break preferentially over the shallower part and then diverge into the deeper trough-channel. This creates longshore currents, that converge in the embayments between the crescents, inducing a wave set up and feeding rip currents back seawards. The flow in the embayment slightly erodes

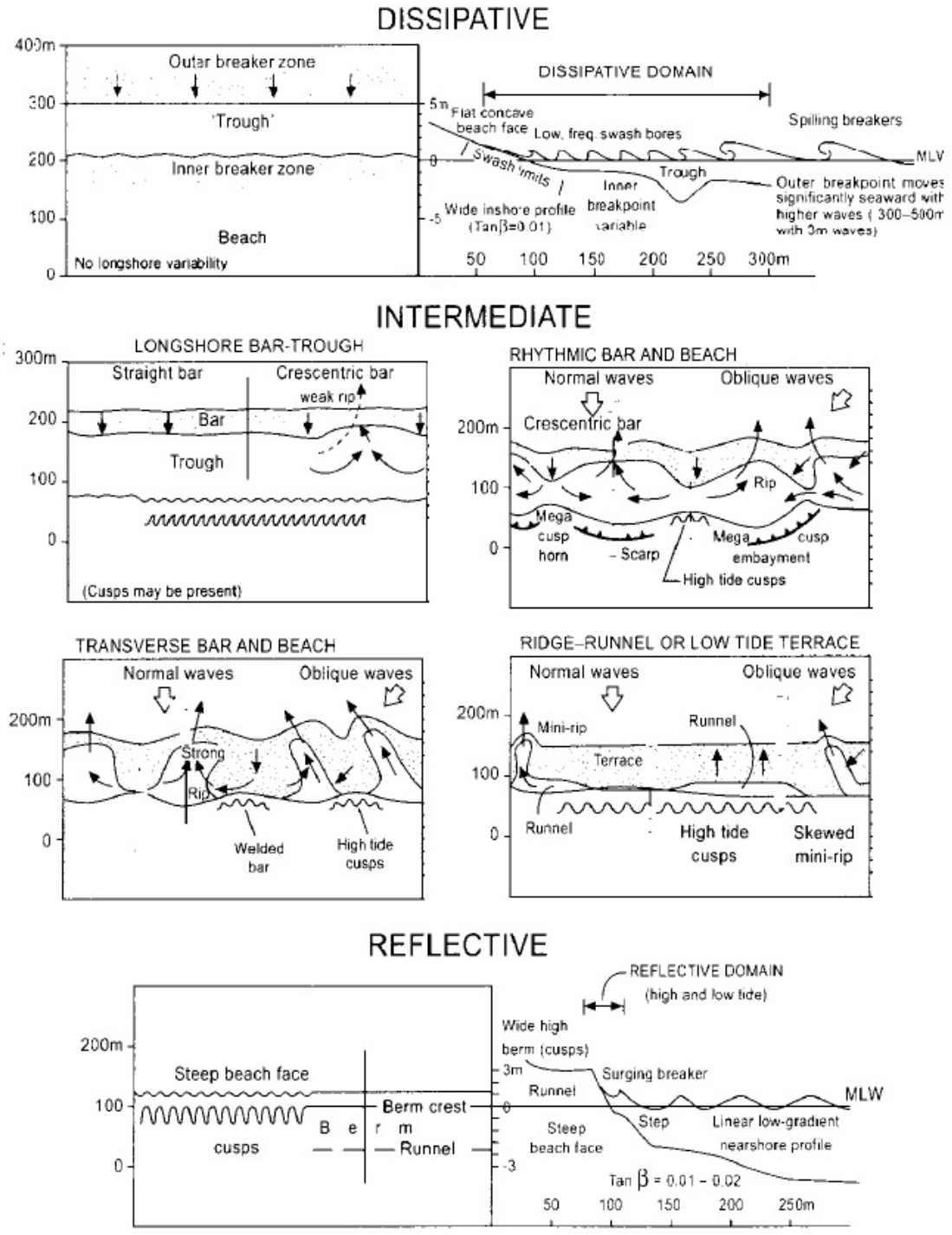

Figure 2.8: Schematic drawings of the bar states as defined by Wright & Short (1984). Figure taken from Short (1999)

sediments, so that seaward-protruding 'horns' mirror the crescentic bars, although in between the longshore trough remains continuous. Rip currents transport sediment away with velocities of 0.5 - 1 ms^{-1}

When the crescentic bars become attached to the shore the beach state is called 'transverse bar and rip' (TBR). The surf zone and beach comprise the longshore alternation of shallow transverse bars and deeper embayments with rip currents. The last intermediate state before the reflective end is the 'low tide terrace' (LTT). These do not have a rhythmic topography anymore; except for some small remains of rip channels a flat longshore bar is attached to the low tide level of a moderately steep beach face. Price & Ruessink (2011)

The state description is often only temporary valid. The nearshore is very mobile: onshore or offshore migration of the parallel bars and changes take place on timescales of days to weeks. A beach will therefore continuously evolve from one state towards another. The state sequence can go in two directions: A 'downstate' sequence implies accretion from the dissipative state towards the reflective state. In this sequence the bars and nearshore zone evolve successively through the intermediate states. The longshore bar will gradually move shoreward, becoming ever more undulated, and eventually merge with the shoreline. Upstate sequences imply erosional processes, often related to storm events. The alongshore bar will then be pushed seaward again. In an accretionary sequence the alongshore bar will in general pass through the intermediate states one by one. However, since erosion is often caused by a relatively violent change in weather / wave conditions, in a downstate sequence the bar will not progress through all the intermediate states.

The bar state model by Wright & Short (1984), was originally developed for single-barred beaches. On swell coasts, like the Gold Coast, two or even three shore-parallel bars are very common. Short & Aagaard (1993) devised that the state model is also applicable for double-barred beaches; each of the bars can go through the described states. In general the outer bar (most seaward bar) is in a higher state than the inner bar, the inner bar being more dynamic anyway. In a double barred shore system, the important influence of morphological feedback between the outer and inner bar adds up to state dynamics that are mostly dependent on the wave climate (Price & Ruessink (2011), Almar *et al.* (2010)). The sequence of states therefore is somewhat more complex. In the study to the alongshore bar system at Surfer's Paradise beach Price & Ruessink (2011) introduce two additional intermediate states: the 'erosional transverse bar and rip' state (eTBR) and the 'rhythmic low tide terrace' (rLTT). The eTBR-state represents the erosional situation of a lower state, occurring when the wave incidence angle is relatively large. It is characterised by a bar that is more or less longshore uniform, while the trough is still discontinuous, with obliquely orientated rip channels in it. The rLTT state is a terraced surf zone, on which a rhythmic alongshore bar line is present. This state is typical for the inner bar, and thought to be the result of interaction with the outer bar when it is in a transition to or from the TBR state.

3 Material and Methods

3.1 Observations at Surfers' Paradise beach

3.1.1 Study site

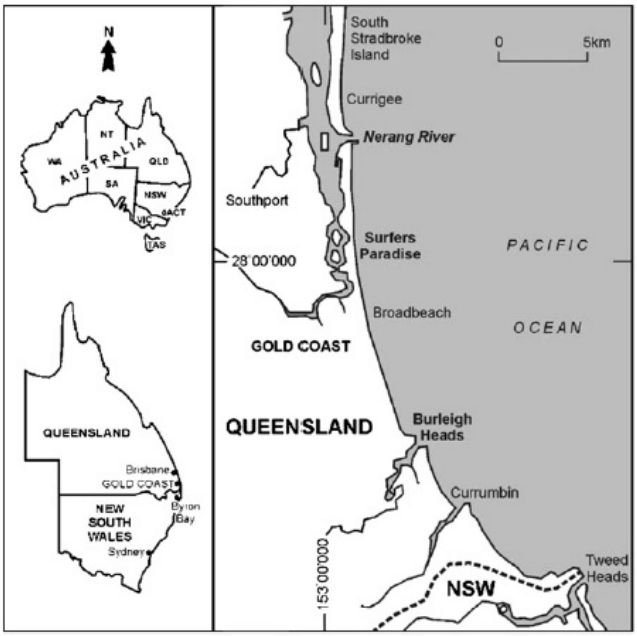

Figure 3.1: Location of Gold Coast and the study site Surfer's Paradise beach (image copied from Price & Ruessink (2011))

The data used in this study are observations of a beach called 'Surfer's Paradise', located on the Gold Coast, in the south-east of the state of Queensland, East-Australia. The Gold Coast consists of a series of quite narrow, stretched barrier islands, densely occupied by (tourist) residences. At the eastside, where the barriers are exposed to the Pacific ocean, long sandy beaches are found. The coastline is aligned approximately North-South. Surfers Paradise beach is a 20 kilometers long, more or less continuous stretch of beach, extending from Burleigh Heads in the South to the outfall of the Nerang River in the north. The study site is a 3 kilometers long stretch of coastline, at the northern end of this beach, see figure 3.1.

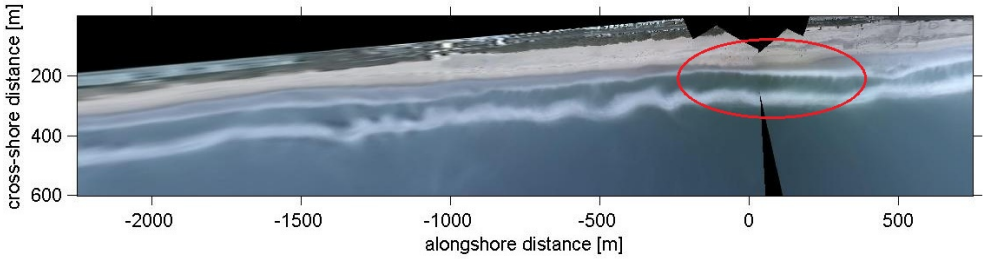

Figure 3.2: An example of an ARGUS image on which within the red encircled zone a patch of transverse finger bars was observed. On this image the coastline (west) is located at the top of the image.

3.1.2 Argus video images

The most important observations of the study site are the ARGUS images. The ARGUS coastal imaging system is applied in over 20 locations, all over the world, e.g. East coast USA, the Netherlands, Spanish Mediterranean, (...). It consists of four cameras positioned at a high place, pointing at different angles. During daylight hours the cameras take snap shots of the beach and nearshore zone. The images of the four cameras are merged together to cover a view angle of 180°. Rectification of the image fits the oblique image on a regular grid, that permits quantitative analysis of the observed zone. For most analysis 'time-exposure' images are used; these are the 10-minute averaged images composed out of snap shots taken at a frequency of 1 Hz . The averaged image permits to distinguish the areas of the nearshore where foam from breaking waves is always present. Especially the images taken around the daily low tide show the breaker areas. Permanently foamy areas are a strong indicator of the presence of sandbars.

The ARGUS system at Gold Coast is installed on top of a 100m. high apartment building, next to Surfer's Paradise beach. With the camera position as the zero-coordinate, the obtained planview images give a view 2500 m. southward and 2500m. northward along the coast, spanning 900m. in offshore direction. The data used for this study is a 9.3-year series of ARGUS images, the observation period spanning from 15 July 1999 until 29 October 2007. For this project 4 years of this series is analyzed: 1 November 1999 to 31 October 2003. This period is chosen while it centers around the dates of the bathymetric information. Moreover the choice of the exact dates is based on the classification of the Queensland Environmental Protection Agency (EPA). In EPA's annual Wave Report (Mohoupt *et al.* , 2004) the Australian summer is classified to extend from 1 November to 30 April and winter is considered to be from 1 May to 31 October. The study period therefore covers exactly four summer and winter seasons. For each day in this period the four images around daily low tide are scanned for the presence of small break lines with a transverse orientation to the coast. The studied images do not cover the whole ARGUS-system field, but focus on a 3.0 kilometers alongshore stretch, 2250 m. south and 750 m. north of the camera position, 600m. in offshore direction. The accuracy of the images is about one pixel, so 1m. Towards the end of the images, especially the southern end, the accuracy worsens to something in the order of 10m. Figure 3.2 shows an example of a planview image, exactly covering the study site. Encircled is a series of transverse break lines in the inner surf zone, interpreted as a transverse finger bar event.

3.1.3 Wave data

Information about the wave climate at Surfer's Paradise is derived from data from two wave recording series, one from a buoy offshore Gold Coast, one located near Brisbane, 76 kilometers more North. The Gold Coast buoy is located in water with a depth of approximately 18 meter, 1 to 2 kilometers from the beach. It has been deployed since February 1987, in association with projects of beach nourishment and the construction of an artificial wave breaker reef before the coast of Surfers Paradise (located on the northern edge of our study domain). The buoy provided a series of hourly averaged values of the root-mean-square wave height, $\widehat{H}_{rms}$ and the peak wave period, $\widehat{T}_{peak}$ (tildes indicate offshore value of the parameter). The Brisbane wave rider buoy is located further offshore, in 80 meters depth. It has been deployed since November 1976. In contrast to the Gold Coast buoy, it is directional, providing a series of hourly averaged values of the incoming wave angle, $\widehat{\theta}$. The directional information used is the angle with respect to the shore-normal. Positive values indicate that waves are coming in from the east to the south; negative values indicate waves from theeEast to the north. The wave angle measured at the Brisbane buoy is transformed to a value that is valid at 18 m-depth, by means of Snell's law of refraction

Apart from directional information the Brisbane wave recordings are used to fill up eventual measurement gaps in the Gold Coast wave rider buoy recordings. For this a neural network is used (see Ruessink *et al.* (2009)).

3.1.4 Bathymetric data

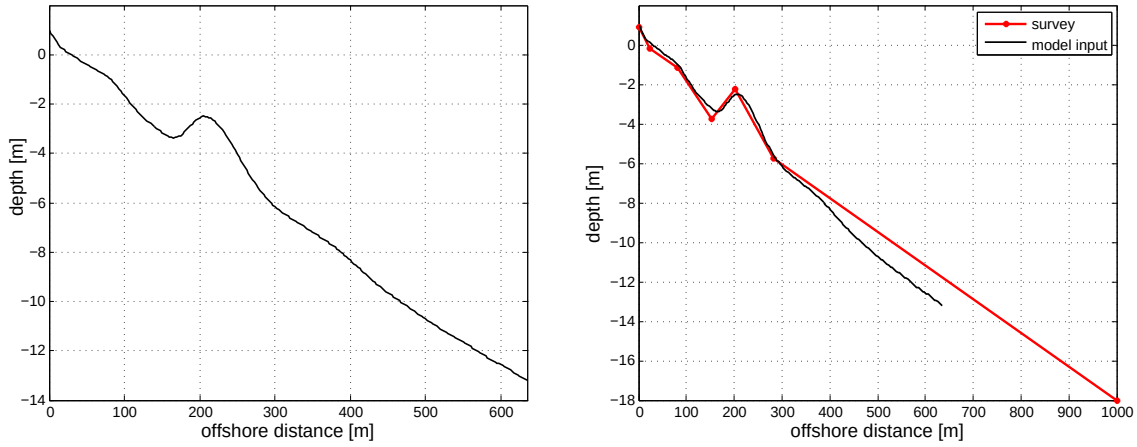

Figure 3.3: left: Bathymetry profile at alongshore coordinate $y = -600m.$ that resulted the bathymetric survey of Surfer's Paradise beach on 12 June 2002. Profile extends from the +1m. beach level to about 600m. offshore; right: In red the schematic topography used as input to the model, which is made up of 7 coordinates only, based on the survey bathymetry of 12 June 2002 (black line), with a linear extension to $1000m.$ offshore where the depth is $-18m.$.

Around Surfer's Paradise beach various bathymetric surveys have taken place. Unfortunately only two of these surveys between 1999 and 2004 also covered this project's study site. It concerns a survey on 28 February 2001 and another one taken on 12 June 2002. The measurements extend

from the backside of the beach seaward to about 800 meters offshore. The measured profiles are interpolated on a regular square 2.5 meter XY-grid. A colour maps of the interpolated bathymetry of the 12th of June 2002 is shown in figure 3.4. However, there are no transverse finger bar events observed close in time to the 2001-bathymetric survey which puts some doubts to its usability in our research. Fortunately there is a developed event observed from 7 to 9 June 2002. The general shape of the nearshore morphology on the date of the survey seems not to differ very much from the morphology during the event. The event is located around 600 meter South of the camera position. A line drawn here from the depth = $+1m$.- level on the beach seaward results the bathymetric profile shown in the left subfigure of figure 3.3. The nearshore zone is characterised by an outer alongshore bar around 200m. offshore, and an inner alongshore bar at approximately 100m. offshore. From the profile it can be concluded that this inner bar is almost attached to the shoreline.

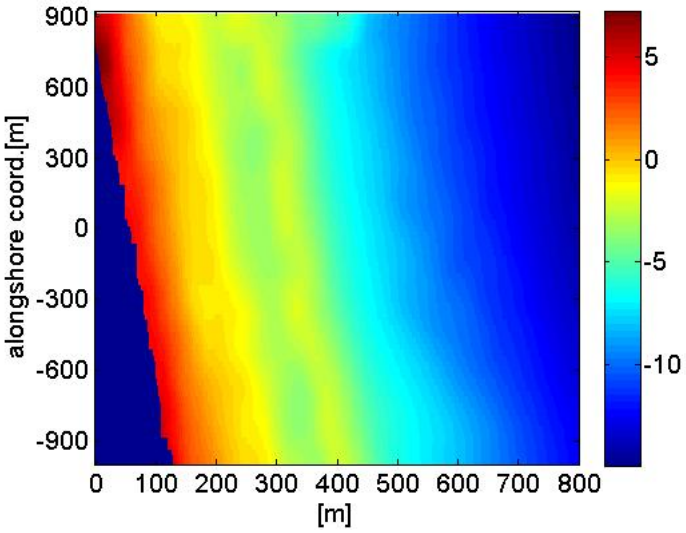

Figure 3.4: Colour map of the bathymetry as determined in the survey of 12th June 2002, colours representing the water depth. Top of the image is the north side, so the beach line is the dark blue side on the left part of the image, whilst the sea extends towards the right.

.

3.2 The morfodynamic model: MORFO62

The model MORFO62 is a process-oriented model, describing the feedback between currents, waves, the free surface evolution and the bed evolution in the nearshore zone. It is a 2DH model, since alongshore homogeneity is assumed. The model makes use of depth-averaged equations. The model MORFO60 (Calvete *et al.* , 2005) forms the basis for MORFO62. The original model is extended with equations describing the roller dynamics of breaking waves and an extra term in the sediment transport formula, representing the effect of the rollers on sediment resuspension. This extension has proven necessary for a realistic model result of the hydrodynamics in the nearshore zone and to model crescentic bars and transverse finger bars (Ribas *et al.* , 2011b).

The (Cartesian) coordinate system is shown in figure 3.5. The x-axis points in seaward direction, the y-axis northward along the uniform, linear coastline. The z-axis points vertically

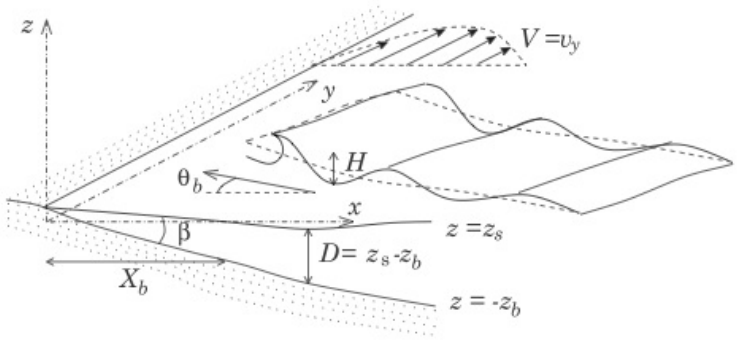

Figure 3.5: coordinate system of MORFO62. Here x and y are the cross-shore respectively the longshore horizontal coordinates, z is the vertical coordinate. The total water depth D depends on the location of the sea bed and the water level. Waves approach the shoreline under an angle θ, thus inducing a current V along the shoreline. Wave height H is the vertical distance between crest and trough level of a wave.

upwards, where z_b is the height of the seafloor and z_s the height of the water surface. The total water depth D can then be defined as $D = z_s - z_b$, in which z_s is the water surface location and z_b the sea bed location.

3.2.1 Model equations

Here, the equations of the complete MORFO62 model are presented. The indexes i, j can have the values $1, 2$ everywhere.

Hydrodynamics

The fluid motions are governed by a continuity equation and a momentum balance, which both are wave and depth averaged. Quasi-steady conditions are assumed, so that all time-derivatives are zero. Wave motion is an important component of the total flow. The waves are assumed to evolve as linear shallow water waves from the offshore boundary to the coast, described by equations (2.2), (2.3) and (2.4).

Continuity:

$$\frac{\partial D}{\partial t} + \frac{\partial}{\partial x_j}(Dv_j) = 0. \tag{3.1}$$

Momentum:

$$\frac{\partial v_i}{\partial t} + v_j \frac{\partial v_i}{\partial x_j} = -g\frac{\partial z_s}{\partial x_i} - \frac{1}{\rho D}\frac{\partial}{\partial x_j}(S_{ij}^w + S_{ij}^r - S_{ij}^t) - \frac{\tau_{bi}}{\rho D} + \frac{\tau_{wi}}{\rho D}. \tag{3.2}$$

Herein $\vec{v} = (v_1, v_2)$: depth-averaged current , D : depth , z_s : surface waterlevel , ρ: water density, $S_{ij}^w, S_{ij}^r, S_{ij}^t$: resp. radiation stresses due to wave propagation and roller propagation and turbulent Reynolds stresses. τ_{wi} is the wind induced shear stress. Wind is not taken into account in this study. Finally τ_{bi} are the components of the bed stresses.
The bed shear stresses are parameterized following a 2D-extension of the formulation by Feddersen *et al.* (2000):

$$\tau_{bi} = \rho c_D \frac{u_{rms}}{\sqrt{2}} v_i \Big(1.16^2 + 2\frac{|\vec{v}|^2}{u_{rms}^2}\Big)^{\frac{1}{2}}. \tag{3.3}$$

Here the factor c_D is the bed drag coefficient, which is parameterised by the often used Manning-Strickler law:

$$c_D = 0.015\Big(\frac{k_a}{D}\Big)^{\frac{1}{3}}. \tag{3.4}$$

In this expression k_a is the apparent bed roughness. Further there is the wave orbital velocity in equation (3.3), u_{rms}. In shallow water the orbital velocity has a strong horizontal component, bringing about linear motions:

$$u_{rms} = \frac{H_{rms}}{2}\frac{g}{c}\frac{\cosh|K|z_0}{\cosh|K|D}. \tag{3.5}$$

z_0: bed roughness length
The concept of radiation stresses was already presented in paragraph 2.2. Two types are distinguished: Wave radiation stresses S_{ij}^w and roller radiation stresses S_{ij}^r. Next to those the turbulent Reynolds stresses S_{ij}^t are taken into account, that describe the transfer of momentum from turbulent eddies to the flow. The following formulations are used in the model:

Wave radiation stresses:

$$S_{ij}^w = E\Big(\frac{c_g}{c}\frac{K_i K_j}{K^2} + (\frac{c_g}{c} - \frac{1}{2})\delta_{ij}\Big). \tag{3.6}$$

Roller radiation stresses:

$$S_{ij}^r = 2E^r\frac{K_i K_j}{K^2}. \tag{3.7}$$

In the above equations (3.2) (3.6) (3.7):
c : wave phase velocity, c_g : group velocity
K_i, K_j: components of the wavenumber κ (see paragraph 2.2).
δ_{ij} : dirac-delta function; 0 if $i \neq j$

The cross-shore component of the radiation stresses depends on the square of $\cos\theta$, the long-shore component is a function of $\sin(\theta)\cos(\theta)$, θ being the angle of the waves with respect to the shore-normal.

Turbulent Reynolds stresses:

$$S_{ij}^t = \rho\nu_t D\Big(\frac{\partial v_i}{\partial x_j} + \frac{\partial v_j}{\partial x_i}\Big). \tag{3.8}$$

ν_t : turbulent diffusivity; formulation of Reniers *et al.* (2004) is used:

$$\nu_t = M\Big(\frac{D^r + (1-a_{roll})D^w}{\rho}\Big)^{\frac{1}{3}} D. \tag{3.9}$$

Here M : turbulence parameter of order 1, D^r: roller dissipation, α_{roll} the fraction of the breaking wave energy dissipation that is transferred into surface rollers.

In linear wave theory, the wave energy is a function of the square of the wave height. Here H_{rms} is used as the typical height of the wave field:

$$E = \frac{1}{8}\rho g H_{rms}^2. \tag{3.10}$$

Wave energy balance:

$$\frac{\partial E}{\partial t} + \frac{\partial}{\partial x_i}\big((v_i + c_{gi})E\big) + S_{ij}^w \frac{\partial v_j}{\partial x_j} = -D^w. \tag{3.11}$$

Roller energy balance:

$$\frac{\partial(2E^r}{\partial t} + \frac{\partial}{\partial x_i}\big(2(v_i + c_i)E^r\big) + S_{ij}^r \frac{\partial v_j}{\partial x_i} = -D^r + \alpha_{roll} D^w. \tag{3.12}$$

The wave energy propagates with the wave group velocity, c_g, whilst for propagation of the roller energy it is the wave phase velocity c.
In the above equations D^w and D^r are the energy dissipation rates due to respectively wave breaking and the rollers. These terms are mostly parameterized and a variety of formulations exists in literature. For the wave energy dissipation rate, the model uses the standard formulation by Thornton & Guza (1983):

$$D^w = \frac{3B^3\rho g\sigma H_{rms}^5}{32\sqrt{\pi}\gamma_b^2 D^3}\Big(1 - \Big(1 + \big(\frac{H_{rms}}{\gamma_b D}\big)^2\Big)^{-2.5}\Big). \tag{3.13}$$

Herein is B an (O)1 parameter that describes the type of breaking. γ_b is the saturation value or breaking index; the value of H_{rms}/D for which shoaling waves are expected to break. For D^r the formulation as used in Ruessink *et al.* (2001) is taken:

$$D^r = \frac{2gE^r sin\beta}{c}. \tag{3.14}$$

In this expression β: slope of the wave front; parameter of $O(10^{-1})$

Sediment transport and bed evolution

The change of the sea bed level z_b as a result of the sediment transport by the water is described by the bed evolution equation:

$$\frac{\partial z_b}{\partial t} + \frac{1}{1-p}\frac{\partial q_i}{\partial x_i} = 0. \tag{3.15}$$

p is the porosity of the seabed, q_i are the components of the volumetric sediment transport, the volume $[m^3]$ of sand grains moving through the watercolumn per unit width of bed $[m]$ and per unit of time. Most sediment transport formula are semi-empirical formulas Here the commonly used model by Soulsby (1997) forms the basis. It calculates the sediment flux, q, as a function of the wave and depth averaged current v_i, distinguishing the suspended load transport and the bedload transport.

$$q_i = G\Big(v_i - \Gamma\frac{\partial z_b}{\partial x_i}\Big). \tag{3.16}$$

G represents a sediment stirring function. A variety of these exist in literature. Soulsby (1997) uses

$$G = A_s[F' - u_{crit}]^{2.4} \qquad \text{if} \quad F' > u_{crit}; \quad G = 0 \quad \text{otherwise.} \tag{3.17}$$

Here A_s is a parameter formed by the sediment properties, mainly the grain size of the sand. It has a component for both the suspended load and the bed load sediment transport.
Suspended load:

$$A_{ss} = \frac{0.012 d_{50} D_*^{-0.6}}{[(s-1)g d_{50}]^{1.2}}. \tag{3.18}$$

Bedload:

$$A_{sb} = \frac{0.005 D (d_{50}/D)^{1.2}}{[(s-1)g d_{50}]^{1.2}}. \tag{3.19}$$

Total load:

$$A_s = A_{ss} + A_{sb}. \tag{3.20}$$

Herein is d_{50} the median grain size and D_* the dimensionless grain size:

$$D_* = \Big[\frac{g(s-1)}{\nu^2}\Big]^{1/3} d_{50}. \tag{3.21}$$

In this expression ν: kinematic viscosity of water, $1.36 \times 10^{-6} m^2 s^{-1}$, s: relative density of the sediment. u_{crit} is the critical velocity the water current should be to stir the sediment loose. The term F' is the stirring velocity. In the original Soulsby van Rijn model it is formulated as

$$F' = (|\vec{v}|^2 + 0.018 c_D^{-1} u_{rms}^2)^{1/2}. \tag{3.22}$$

This equation describes that sediment stirring is determined by both the current velocity as by the orbital velocities induced by wave propagation. In MORFO62 an extension of this formulation is used, adding the contribution of turbulent eddies from the roller dissipation to the total sediment stirring, as done before by Reniers *et al.* (2004). The term F' is extended with a term for the turbulent velocity of the vortices, u_{bor} and a parameter, n_{bor}, determining the strength of the sediment resuspension by roller-induced turbulence:

$$F' = \Big(|\vec{v}|^2 + 0.018 c_D^{-1} u_{rms}^2 + n_{bor} u_{bor}^2\Big)^{1/2}. \tag{3.23}$$

$$u_{bor}^2 = \Big(e^{(D/H_{rms})}\Big)^{-m_{bor}} \Big(\frac{D^r}{\rho}\Big)^{2/3}. \tag{3.24}$$

Then in equation (3.16) the Γ is the 'global bedslope coefficient', expressing the slope effects on the sediment transport. One way to formulate it is

$$\Gamma = \gamma(F' - u_{crit}). \tag{3.25}$$

where the parameter $\gamma = 0.6$.

In summary there are five variables to solve the equations for: $z_s(x, y, t)$, $z_b(xyt)$, $\overrightarrow{v}(x, y, t)$, $E(x, y, t)$, $E^r(x, y, t)$ and $\Phi(x, y, t)$, the wave phase. The boundary condition is that there is no flow at both the offshore boundary ($x \to \infty$) and at the coastline ($x = 0$). On the seaward edge of the domain monochromatic waves with a specific waveheight $\widehat{H}_{rms}$, wave period $\widehat{T}_{peak}$ and angle with respect to the shore normal $\widehat{\theta}$ are prescribed. These wave conditions and all other parameters used in the model equations are listed in appendix B. Also the initial steady sea bed profile is described. Input to the model is a topography based on the bathymetry profile following the 2002-bathymetric survey of Surfer's Paradise beach. To facilitate the model, this profile is schematised into a 7-coordinates (x, z) topography. This is shown in the right panel of figure 3.3. The simplified topography describes the location of the shoreline and the crests of the alongshore bars accurately. The bathymetry survey only extended to 600 m. offshore. Since the wave conditions are prescribed at 1000 m. distance, the input-topography is further extended with a slope to this domain limit and 18 m. depth.

3.2.2 Model implementation

Methodology

The hypothesis that transverse finger bars form by self organization processes, is tested by means of a linear stability analysis. A linear stability model is a simplified version of full numerical process-oriented models. Here the physics is focussed on the initial growth rate and shape of the appearing bed forms. It is a useful method for optimization of parameters, sensitivity studies and just to improve understanding about the causes of bed form formation. Note that this type of model is not able to describe the long-time predictions of morphological evolution.
Out of the system of equations, the momentum and energy balance and the sediment transport versus the bed level evolution equation, first a basic state is determined. The basic state represents the morphodynamic equilibrium between waves, currents and sea bed in the nearshore zone, in which the net cross-shore sediment transport is zero. It describes the equilibrium values of the different variables with respect to a steady bed-topography profile; the basic state is stationary and alongshore uniform. Subsequently, in the linear stability analysis (LSA) can be applied: a small, alongshore periodic bottom perturbation with an arbitrary distance, the wavelength λ or wavenumber $\kappa = \frac{2\pi}{\lambda}$ are added to the basic state equilibrium values of the variables. Next to being stationary, the basic state is assumed to be homogeneous in the alongshore (y) direction. For the bed level this reads:

$$z_b(x, y, t) = z_b^o(x) + \mathfrak{Re}\big(e^{\omega t + iky} h(x)\big). \tag{3.26}$$

Similar expressions are used for the other dependent variables of the system of equations, z_s, v_1, v_2, E, E^r and Φ. The perturbations are assumed to be very small when compared to the basic variables. Therefore after inserting the expressions into the governing equations, linearization with respect to the perturbations can be done. This results an eigenvalue problem: for each arbitrary perturbation, sized κ, different eigenvalues ω_n exist, characterizing the different possible growing modes n. ω_n can be split up into a real and an imaginary part, $\mathfrak{Re}(\omega) = \Omega$ and $\mathfrak{Im}(\omega)$. The real part represents the growth rate of the perturbation, for $\Omega > 0$ the solution is

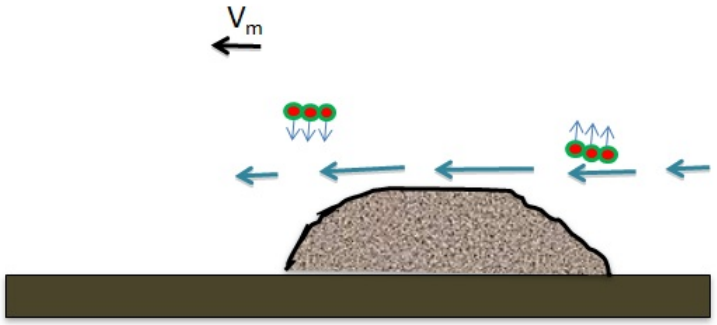

Figure 3.6: Schematical drawing illustrating the migration of a sand bar. Due to flow divergence over the bar, sediments get eroded at the upstream side of the current (V_m). Downstream of the bar flow convergence result in sediment deposition again. This way the bar will gradually move in the direction of the mean current, with migration rate C.

growing in time. In this case convergence of flow (sediment transport) takes place on the crest areas of the bed perturbation. For $\Omega < 0$ the basic state is stable. Around the initially formed sediment crests sediment transport diverges, such that the perturbation will dampen again.
When the developing bar has a certain size, it may influence the flow dually; flow divergence over the crest together with flow convergence over the trough induce erosion on the up-current side of the bar, sediment deposition at the dow-current side. This way the sand bar will slightly migrate in the direction of the main flow. This process is illustrated in figure 3.6

$\mathfrak{Im}(\omega)$ is used to calculate the phase speed of the perturbation, the migration rate of the bars:

$$C = \frac{-\mathfrak{I}(\omega)}{\kappa}. \tag{3.27}$$

The first model runs are based on a default setup, considering the waves and other model parameters. To best represent the Gold Coast beach, the default values are based on the wave conditions typical for the observed transverse finger bar events. Than this basic state is perturbed with a series of bottom perturbations sized κ. Not all these perturbations will result in instability. From the ones that do, it is assumed that one specific will finally dominate the system. This is the perturbation associated with the highest growth rate Ω_{max}, having the preferable wavelength $\lambda_{pref} = 2\pi/\kappa_{pref}$ and migration rate $c_{pref} = -\mathfrak{I}(\omega_{max})/\kappa_{pref}$.

The value of Ω_{max} may be sensitive to the characteristics of the incoming waves, the partition of the wave energy into dissipation and rollers and the strength of the rollers in general. In the linear stability analysis the sensitivity to the wave and model-parameters on Ω_{max}, the preferred perturbation size, k_{pref}, and the corresponding migration rate c_{pref} can be tested.

Numerical implementation

The full set of differential equations is solved by means of a spectral collocation method: the solution of the system is approximated by a linear combination of continuous functions that are generally nonzero over the domain. Here for these 'trial functions' Chebyshev polynomials are used. These are defined on [-1,1] by

$$T_k(x) = \cos(k \cos^{-1} x). \tag{3.28}$$

for $k = 0, 1, ...$ where $T_k(x)$ are the trial functions. The domain is divided in collocation points. On each point of the grid (x_n) the approximate solution, made up of the truncated series of polynomials, agrees exactly with the original differential equation. The collocation points do not have to be equally spaced, but can be distributed arbitrarily. This way the level of accuracy can be varied over the domain. The collocation points can be distributed over the computational domain such that there is a focus on the zone where variations are most rapid: the surf zone region close to the shore (see Calvete *et al.* (2005)). To prescribe the numerical grid, MORFO62 uses four parameters that can be varied in the input file: the number of collocation points NX, the distance from the lower domain limit within which half of the points is located, OL, a factor that stretches the grid in the middle of the domain, OA, and another stretching parameter, OS, that can bring the outer limit of the domain a bit closer.

4 Results

4.1 Analysis of the observations of Surfer's Paradise beach

4.1.1 Transverse fingerbar events

At first the results concerning the analysis of the observations of Surfer's Paradise beach, the ARGUS images and the wave buoy data, will be presented, in order to answer the questions about the typical characteristics of the transverse finger bars at the Gold Coast. The data set of Argus-images from the period 1 November 1999 until 31 October 2003 is an almost continuous series of images: for 1430 days in total, there are only 59 days of which we do not have any images of the beach. For every day of the study period, the three or four images around daily low-tide have been analyzed visually, tracing the occurrence of transverse finger bar events, their duration, the number of bars per event, and the average spacing between the bars in a patch (the wavelength). The occurrence of transverse finger bars is considered an event when on one location 3 or more bars are visible for 2 or more days in a row. The variety in number of bars and duration is large, which made us decide to divide the events in three classes: '0'-events contain only 3 bars or are only visible for 2 days; '1'-events, or 'developed' events, contain 3 bars for a longer duration, or more bars for only 2 days; '2'-events, or 'well developed' events, consist of 4 or more bars for 3 or more days. Unfortunately not all the images were as clear, neither were all the bars always well defined. During these four years, from the start of summer in 1999 to the end of winter 2003, 69 events are distinguished, of which 26 'developed' events (class 1) and 35 events are considered 'well developed' (class 2). On average there are 17 events per year with a peak of 24 events between November 2000 and October 2001.
On Duck beach there was a clear seasonal variability in transverse finger bar occurrence, with few trough bar events observed in summer (Konicki & Holman (2000)). At Gold Coast however there is not a clear seasonal signal in the transverse finger bar presence: table 4.2 shows the division of events over summer and winter: there are slightly more events in the East Australian winter than in the summer, but the difference is insignificant. In total there were 349 days with finger bar patches, hence at Surfer's Paradise beach transverse finger bars are present during 24% of the time. Both the duration of an event and the number of bars per event are quite variable: the minimum duration observed is by definition 2 days, whilst in March-April 2003 an event lasted for 21 days. The average duration is about 5 days (median: 4 days). The minimum number of bars per patch is 3, the maximum number observed is 15 bars, occurring in an event from 11- 13 July 2000. The average number of bars per patch is 6 (median value: 5 bars). To determine the average wavelength (the inter-bar spacing), only the class-1 and class-2 events are used, since these best represent the phenomena. This is also done in the analysis of the antecedent wave conditions, presented in the next paragraph. Figure 4.1 shows a typical transverse finger bar event, with 5 up-current oriented bars which were visible for 4 days. From a grayscale image of the original color image the average wave length between the bars in a patch is determined. The

observed wave lengths range from 17 to 71 meters, with an average of 32 meters (median value $\lambda = 31m$.
Appendix A shows the complete list of observed transverse finger bars and their properties.

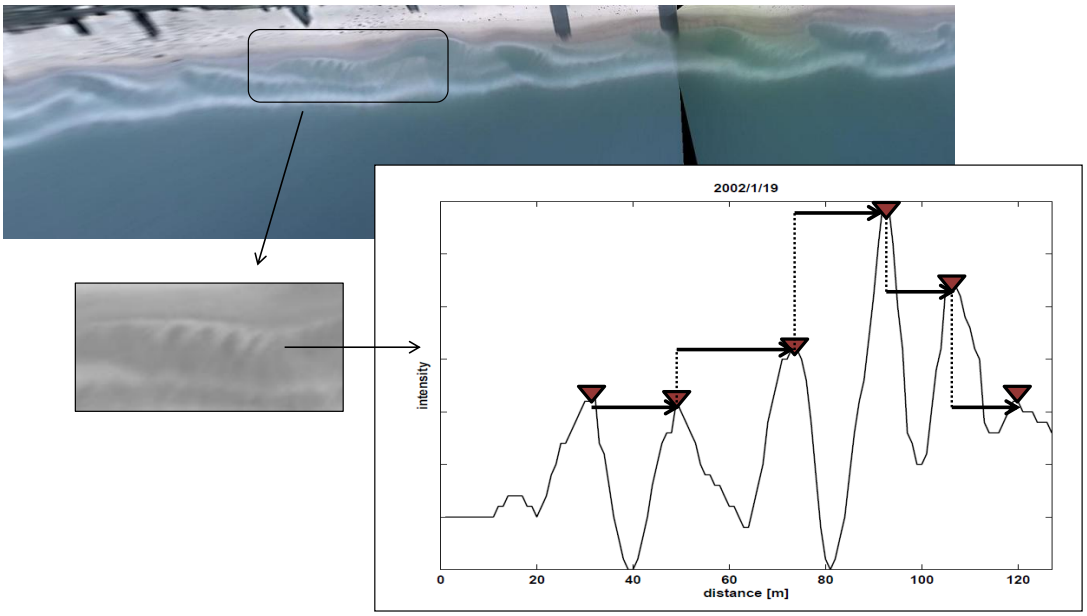

Figure 4.1: Upper: ARGUS image; view from sea shoreward. Here is shown an example of a day with several patches of transverse finger bars. The area in the frame is selected, changed into a grayscale white image, in order to determine the wavelength of the bars by means of an light-intensity plot. Peaks in the intensity correspond to the lightest parts on the image: the finger bar crests. Red triangles in the bottom right graph correspond to crest locations. The average distance between these determines the wavelength

Considering the migration rates, no full analysis is done. Too many events lasted for too short a period to accurately measure the change in position of the finger bars. By the eye the finger bars were never seen to migrate significantly along the shoreline.

4.1.2 Typical wave conditions

For the full study period the offshore wave conditions of the Gold Coast, $\widehat{H}_{rms}$, $\widehat{T}_{peak}$ and $|\widehat{\theta}|$, are determined, based on the information from the Gold Coast and Brisbane wave rider buoys. Of each of the parameters the range, the average value and the standard standard deviation from this average are determined. The range of wave conditions is quite big, with $\widehat{H}_{rms}$ occurring in a range of 0.2 to 2.86m., $\widehat{T}_{peak}$ (in the following: $\widehat{T}_p$) varying from 3 to 22.5 sec. and about all possible wave angles recorded. The determined average conditions correspond to what is found in literature (Turner *et al.* , 2004; Ruessink *et al.* , 2009; Price & Ruessink, 2011), describing an intermediate energy beach. To assess the question whether transverse finger bar growth is dependent on the wave conditions, the wave buoy data antecedent to the events are regarded. To focus on the most typical events, the 0-events are not considered here. Of each developed and well-developed event the average wave conditions 24-hours before the moment when the transverse

finger bars became visible on the images is determined. Here the ranges are significantly smaller, event-typical offshore wave height lying between 0.3 and 1.2 meter., $\widehat{T}_p$ between 5.5 and 13 seconds. These are the differentiating parameters, showing that, corresponding to literature, transverse finger bars are characteristic of relatively calm, intermediate energy, waves.
The absolute wave angle $|\widehat{\theta}|$ range is still quite large, extending from 1 to 62 degrees. The lower limit of this range is remarkable, since it corresponds to about normal wave incidence, in which transverse finger bars were not expected to grow, following the hypothesis that oblique waves are required for finger bar development. The results of the analysis of the wave buoy data are summarized in table 4.1. The averages calculated for the wave conditions of the whole study period and the event-typical wave conditions turn out to be about the same.

Let's look a bit further to the incoming wave angle, $\widehat{\theta}$ and the orientation of the bar crests. Are the bars consequently up-current? The waves approach the Gold Coast generally under an angle, coming from the South to Southeast. They origin from ocean swells generated by low pressure areas over the Tasman Sea and Southern ocean, East Coast lows and Tropical Cyclones (Splinter *et al.* , 2011). Figure 4.1.2 shows the histogram of the incoming wave direction for the total study period, as recorded by the Brisbane directional wave buoy. As explained already a $\widehat{\theta} > 0$ corresponds to waves from the south to the east, negative values of $\widehat{\theta}$ correspond to waves from eastern to northern direction. Although the wave angle is highly variable, the histogram

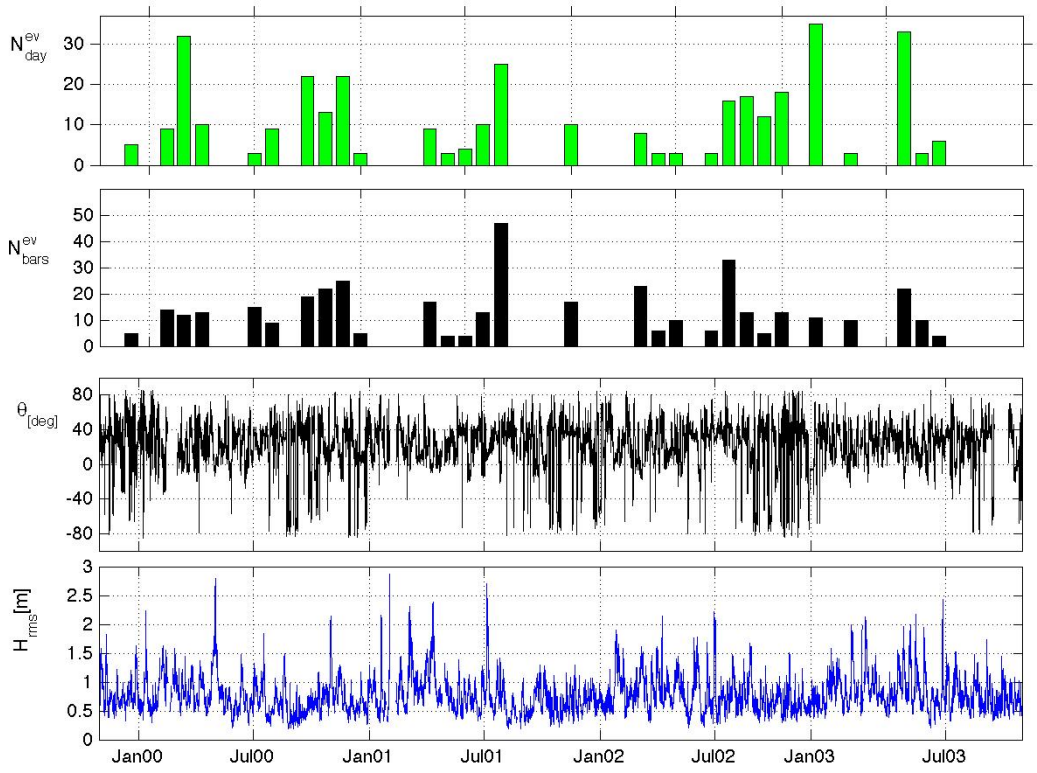

Figure 4.2: Wave conditions at Surfer's Paradise beach during the study period. Upper 2 plots show the monthly variability of transverse finger bars; N_{eve}^{day} is the monthly number of days with events, N_{eve}^{bar} is the total number of bars per month. The lower 2 plots are time series of the daily average $\widehat{T}_p$ and $\widehat{H}_{rms}$.

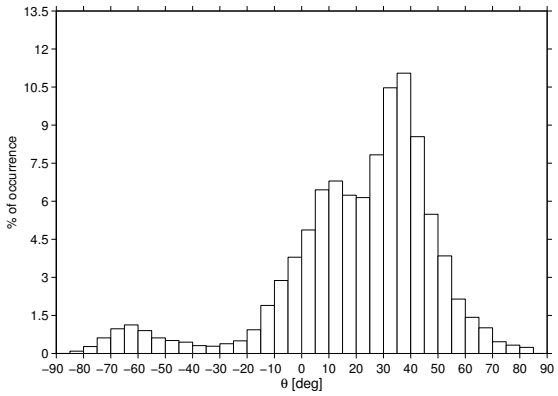

Figure 4.3: Distribution of incoming wave angle over the total study period. $\widehat{\theta} = 0°$ corresponds to the shore normal, which is more or less 'east'; when $\widehat{\theta} > 0\circ$ waves come from southern directions.

indeed shows that the majority of the time the wave incidence has positive values, with a peak-occurrence of waves with a moderate obliqueness, $35 - 40°$. Does this reflect on the orientation of the transverse finger bars? Bars with a crest orientation towards the northeast are observed in 27% of the events, bars with an orientation to the southeast in 71% of the events. In the remaining cases the orientation was more or less normal or not all the bars in a patch clearly pointed in the same direction. Over the whole study period 15% of the time waves from the east to the north are recorded. Looking to the 24-hours before the start of the events with bars pointing to the northeast, far less than half of the events (31%) follow a day with an average $\widehat{\theta} < 0°$. For the events with bars pointing in southeastern direction the correlation to the wave incidence angle is stronger: in 86% of the cases these events follow a day of $\widehat{\theta} > 0$, waves coming into the nearshore zone from the southeast. The correlation for the northeastward orientated bars improves a lot when regarding the offshore incoming wave angle recordings taken during the event. Then during 79% of the events the offshore wave had a northeastern incidence angle. From this one can conclude that the orientation of the bar crests is in the majority of the cases up-current. It is probable that the correlation between incoming wave angle and finger bar orientation is strongest when, antecedent to a transverse finger bar event, the wave angle shows few variability for a longer period of time. This is not further explored here.

offshore wave conditions Nov.1999-Oct. 2003			
	range	average	σ
$\widehat{H}_{rms}[m]$	0.18 - 2.86	0.77	0.32
$\widehat{T}_{peak}[s]$	2.88 - 22.5	9.37	2.48
$\lvert\widehat{\theta}\rvert[\circ]$	0.0 - 85.0	30.0	18.4
wave conditions before start of events			
$\widehat{H}_{rms}[m]$	0.31 - 1.23	0.71	0.20
$\widehat{T}_{peak}[m]$	5.50 - 13.06	9.27	1.78
$\lvert\widehat{\theta}\rvert[\circ]$	1.0 - 62.6	27.5	16.0

Table 4.1: General offshore wave conditions at Gold Coast versus event-typical wave conditions

Class	Summer	Winter
0	3	5
1	12	15
2	18	17
total	33	37

Table 4.2: occurrence of events per season. Summer months are November to April, winter is from May to October

Table 4.3: (Left) occurrence of the different bar states of the outer and the inner bar, in terms of percentage. Upper tabel shows result for the full study period November 1999 - October 2003, with below the bar states observed at the start of the described transverse finger bar events. Right: explanation of the codes used in this table and tables 4.4 and 4.5

Bar state Nov. 1999 - Oct.2003			
Inner bar		Outer bar	
State	% of occurrence	State	% of occurrence
LBT	5.5	D	16.3
RBB	1.9	LBT	19.8
TBR	17.8	eTBR	5.9
rLTT	45.0	RBB	22.7
LTT	13.7	TBR	35.3
R	16.1	-	-
Bar state at start transverse finger bar events			
Inner bar		Outer bar	
State	% of occurrence	State	% of occurrence
LBT	4.9	D	16.4
RBB	1.6	LBT	8.2
TBR	16.4	eTBR	1.6
rLTT	50.8	RBB	23
LTT	14.8	TBR	50.8
R	11.5	-	-

Code	Full name
D	Dissipative
LBT	Longshore bar and trough
TBR	Transverse bar and rip
eTBR	Erosive transverse bar and rip
RBB	Rhythmic bar and beach
LTT	Low tide terrace
rLTT	rhytmic low tide terrace
R	Regressive

4.1.3 Bar state

The alongshore submerged bars in the nearshore zone of Surfer's Paradise beach can be described following the bar state classification by Wright & Short (1984) and Price & Ruessink (2011), as described in section 2.4. Regarding the outer and the inner bar together, all possible states of the alongshore bars are observed during the study period. Only the outer bar sometimes reached the dissipative extreme, the same is valid for the inner bar regarding the reflective extreme.The outer and inner bar are seldom in the same state (in 4% of the days in the total 9.3 year data-set), since the outer bar morphology in general is more upstate, more towards the dissipative side of the bar state sequence, than the inner bar.

To study the relation between the actual bar state and the development of transverse finger bars, the list of bar states is compared to the list of events. More precisely, the actual state of the inner and outer bar at the start of each event is listed. For this result only the events classified as 'developed' and 'well-developed" (the 1-and 2 events) are taken into account, since these best represent the phenomena.
When regarding the bars separately, see table 4.3, it turns out that half of the events develop when the inner bar is part of a rhythmic low tide terrace (rLTT). The outer bar has exactly half of the time a transverse bar and rip configuration (TBR), at the beginning of a transverse finger bar event. Both these peak states belong to a milder wave energy regime. However, as can be read from the upper part of table 4.3, the frequency distribution of the state of the inner bar related to transverse finger bars, is quite similar to the distribution regarding the complete 4-years study period. The rLTT-state is observed in 45% of the time. For the outer bar the distribution of pre-event bar states is a little more different to the multiyear distribution, although the TBR-state is in both cases the preferential state.

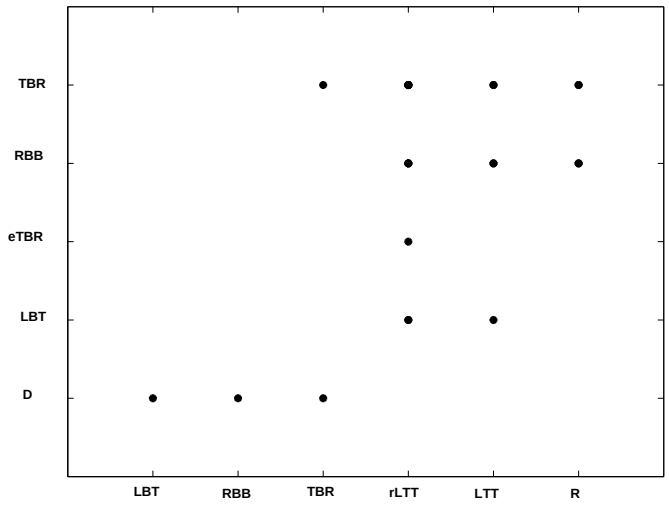

Figure 4.4: Possible combinations of the state of the inner and outer bar

What if we look at the inner and outer bar state simultaneously? Figure 4.4 gives a quick overview which states of the inner and outer bar are seen to occur simultaneously when transverse finger bars can be observed too. Quantitatively table 4.4, but also table 4.5, show that the most

occurring combination of bar states is the simultaneous occurrence of an inner bar in rLTT and an outer bar in TBR; the combination of the two most occurring states. This is both true when regarding the full study period and the days with transverse finger bar events. Figure 4.5 shows the different frequency distributions of the bar state combinations. Peaks in the total occurrence of the different bare state combinations (1999-2003, the dark blue bars), appear as well in the bar state associated to transverse finger bar events. However, the total spreading of bar states is wider than the event-typical distribution. Finger bar presence is preferential to the more downstate longshore bar configurations of both the inner and outer bar.

The transverse finger bars were seen to be attached most often to more straight parts of the inner bar. Sometimes they were located in larger embayments of the outer and inner bar, halfway in between of the place were horns of the outer bar pointed shoreward. But the most observed situation is an undulating outer bar somewhat further seaward, with transverse finger bars attached to longer stretches of a straight terraced inner bar. This supports the hypothesis that the longshore current is an important generation mechanism of transverse finger bars, since the current flows stronger through the trough in between the outer and inner bar Circulation cells, typically developing in an alongshore inhomogenous surf zone e.g. rip current systems, are then less important in finger bar formation.

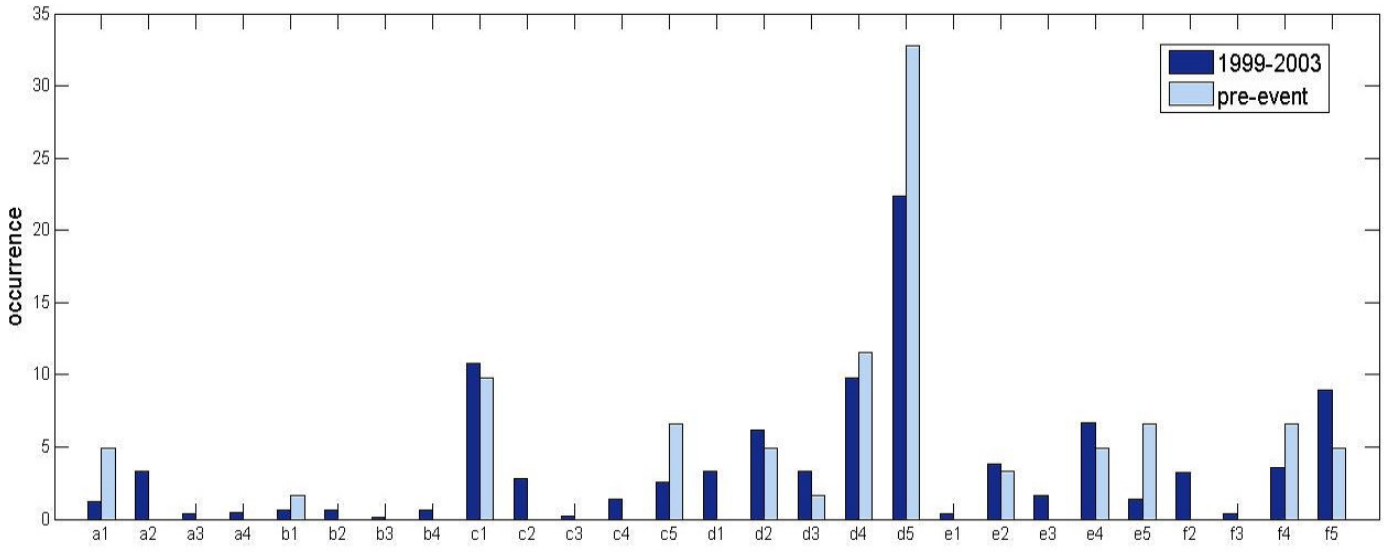

Figure 4.5: Bar plot of the simultaneously occurring states of the inner and outer bar at Surfer's Paradise beach (coding horizontal axis: see table 4.5). In dark blue the frequency of the bar state combinations during the full study period. In light blue the frequency of bar states observed at the start of transverse finger bar events

*	Inner bar	Outer bar	% of occurrence
a1.	LBT	D	5
b1.	RBB	D	2
c1.	TBR	D	10
c5.	TBR	TBR	6.5
d2.	rLTT	LBT	5
d3.	rLTT	eTBR	2
d4.	rLTT	RBB	11
d5.	rLTT	TBR	32
e2.	LTT	LBT	3
e4.	LTT	RBB	5
e5.	LTT	TBR	6.5
f4.	R	RBB	8
f5.	R	TBR	5

Table 4.4: Observed combinations of inner and outer bar state at Surfer's Paradise beach, at the start of the transverse finger bar events, in terms of percentage

*	Inner bar	Outer bar	% of occurrence
a1.	LBT	D	1.2
a2.	LBT	LBT	3.3
a3.	LBT	eTBR	0.4
a4.	LBT	RBB	0.5
b1.	RBB	D	0.6
b2.	RBB	LBT	0.6
b3.	RBB	eTBR	0.1
b4.	RBB	RBB	0.6
c1.	TBR	D	10.8
c2.	TBR	LBT	2.8
c3.	TBR	eTBR	0.2
c4.	TBR	RBB	1.4
c5.	TBR	TBR	2.6
d1.	rLTT	D	3.3
d2.	rLTT	LBT	6.2
d3.	rLTT	eTBR	3.3
d4.	rLTT	RBB	9.8
d5.	rLTT	TBR	22.4
e1.	LTT	D	0.4
e2.	LTT	LBT	3.8
e3.	LTT	eTBR	1.6
e4.	LTT	RBB	6.7
e5.	LTT	TBR	1.4
f2	R	LBT	3.2
f3	R	eTBR	0.4
f4.	R	RBB	3.6
f5.	R	TBR	8.9

Table 4.5: As table 4.4, but then regarding the bar state combinations for the complete 4-years study period., in terms of percentage

4.2 Model results

4.2.1 Default case

Parameter	Meaning	Value
NX	number of collocation points	400
OL	half points position $[m]$	40
OA	stretching parameter 1	0.1
OS	stretching parameter 2	0.95
$\widehat{H}_{rms}$	offshore RMS wave height	0.8 $m.$
$\widehat{T}_{peak}$	offshore wave period	7.5 $sec.$
$\widehat{\theta}$	offshore incoming wave angle	30°
D_{50}	d_{50}; sediment median grain size	$250\mu m$
γ_b	breaking index	0.475
α_{roll}	fraction of wave dissipation in roller energy	1.0
N_{bor}	n-parameter in u_{bor}formulation (ref!)	50.0

Table 4.6: parameters default case MORFO62

Can the model MORFO62 predict the (initial) growth of transverse finger bars from an input that represents the prevailing topographic and wave conditions at the Gold Coast? In order to test this, for the first application of the model a default case is defined. Most typical herein are the wave parameters, the properties of the incoming waves that form the offshore boundary conditions for the model. The default wave parameters lie close to the average wave parameters for the events, as determined in paragraph 4.1.2: $\widehat{H}^{def}_{rms} = 0.8$, $\widehat{T}^{def}_{p} = 7.5$, $\widehat{\theta}^{def} = 30\,\text{deg}$. Table 4.6 shows a table of these and the default values of the other most important model parameters. A complete list of all the parameters used in the default model setup can be found in appendix B. Table 4.6 starts with the four parameters that define the calculation grid, NX, OL, OA and OS, of which the meaning was explained in section 3.2.2. To determine the optimal values of these 'discretization' parameters turned out to be very time-consuming; the model showed a very high sensitivity for the numerical discretization. Varying these parameters does not have big consequences for the basic state result, but it does influence the success of the linear stability analysis. A good combination of the discretization parameters should result in a physically reasonable model-output, that is only changing slowly on changing the input wave parameters. The outcome of the optimization is a very large grid (400 points is the model's maximum), which focusses strongly on the zone near to the beach, since half of the calculation points is located in the first 40m. (OL=40). Default values of OS and OA are chosen such that the calculation grid describes a domain that corresponds well to the domain prescribed by the input topography.
The other parameters in the table are the breaking index γ_b (see equation (2.8)), the median grain size of the sediment d_{50}, and the parameters α_{roll} and N_{bor}. These last two parameters describe the roller dynamics and form the newest extension to the MORFO-model series. α_{roll} is the fraction of the broken wave energy dissipation that is transferred into surface rollers, appearing in equations (3.9) and (3.12). N_{bor} determines the strength of the sediment stirring by turbulent eddies from the dissipating rollers, see equation (3.23). According to Price & Ruessink (2011), Surfers Paradise beachis composed of predominantly quartz sand with a d_{50} of about $250\mu m$. For N_{bor}, α_{roll} and γ_b the default case values are the values used in the modeling of the Duck transverse fingerbars (Ribas *et al.* , 2011a).

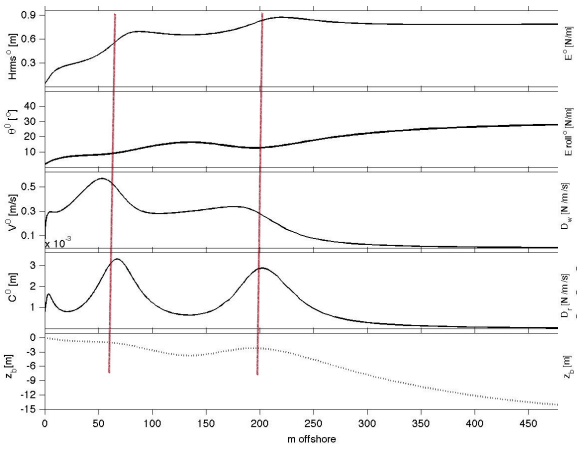

Figure 4.6: Basic state plots for the default setting: wave height H^o_{rms}, wave angle θ^o, longshore current velocity V^o and depth integrated sediment concentration C^o_{di} (^{o} indicates basic state value).

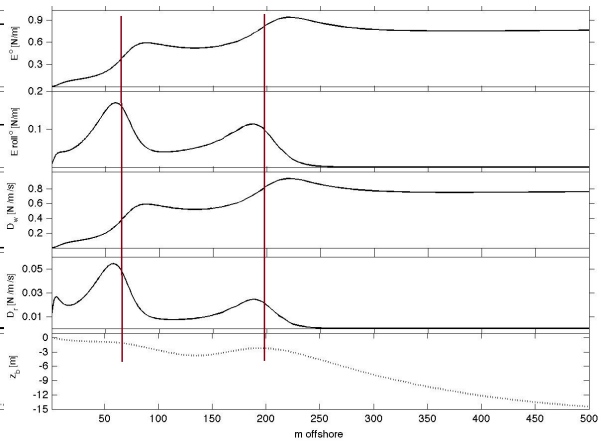

Figure 4.7: Basic state plots for the default case: wave energy density E^o, roller energy density E^o_{roll}, wave dissipation Dis^o_{wave} and roller disipation Dis^o_{roll}.

4.2.2 Basic state

The basic state values are indicated with a superscript, ^{o}. Figures 4.6 and 4.7 show the curves of the wave height H^o_{rms}, wave angle θ^o, alongshore current velocity V^o and the depth-integrated sediment concentration C^o, and the wave energy density E^o, the roller energy density E^o_{roll}, the wave dissipation D^o_w and the roller dissipation D^o_r respectively, in the nearshore 500 meters for the default setting. Bottom plots in both figures show the topography profile, z_b. For clarity red lines are drawn over the figures, indicating the crest location The graphs show the processes in the nearshore zone as they are expected to be: it can be seen that the un-deepening of the water, and especially the presence of the two alongshore bars, effects the hydrodynamics and the sediment transport. . Breaking occurs over the bars and at the shoreline, causing a quick decrease in wave height and energy density here. Accordingly there is a peak in wave energy dissipation D_w just before the bar crests, and peaks in the roller dissipation D_r after these breakpoints. Turbulence caused by the breaking of waves stirs up sediment, so that peaks in the sediment concentration lie around the bar crests and at the shoreline too.

To study the effect of a different model setting on the basic state result a first sensitivity test is done. Sensitivity of the basic state solution to the wave conditions is explored, next to the effect of roller dynamics. The energy of the waves is best represented by the offshore wave height, $\widehat{H}_{rms}$. This input parameter was varied over the range 0.2 - 1.2 meter, of which for three values of $\widehat{H}_{rms}$ the resulting curves are plotted in figure 4.8. Differences in the offshore wave height turn out to have a direct effect on the strength of the longshore current, the amount of wave energy in the system and the intensity of the breaking. Higher incoming waves imply an increase in the total wave energy density and consequently more energy is transferred into the rollers too and more energy will be dissipated. This increase in roller energy density positively affects the intensity of sediment stirring. For lower waves, like $\widehat{H}_{rms} = 0.3m.$ in figure 4.8, few breaking takes place on the outer bar, so that no significant rollers are produced there. More or less the same results follow from the test to the sensitivity to the offshore wave period, $\widehat{T}_p$ (figure

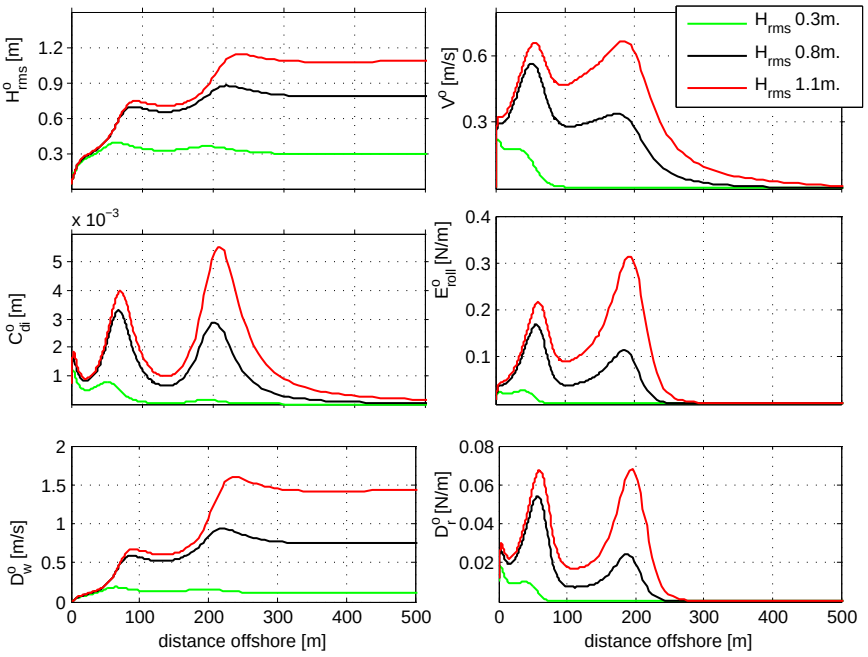

Figure 4.8: Basic state sensitivity: waveheight H^o_{rms}, longshore current V^o, depth integrated sediment concentration C^o_{di}, roller energy E^o_{roll},wave dissipation D^o_w and roller dissipation D^o_{roll} for different values of the offshore waveheight $\widehat{H}_{rms}$.

4.9). An increase in wave period brings about more energy into the system, consequently also wave heights increase. For higher periods more breaking occurs, more energy is transferred into the rollers and more sediment is stirred up around the bar crests and at the shoreline.

Then the effect of the offshore incoming wave angle on the basic state solution is explored. $\widehat{\theta}$ affects the available wave energy. In figure 4.10 it can be seen that the more oblique the waves approach the coast, the less energy there they carry into the nearshore zone. For waves with $\widehat{\theta} = 65°$ the wave energy density at the outer bar is only half of the energy when the waves would approach almost normally with respect to the coast. The roller energy of the very oblique waves over the outer bar is even only 20% of the roller energy here of a normal-incoming wave. This has its effect on the sediment stirring, which is 60% less for waves with $\widehat{\theta} = 65°$ than for waves with $\widehat{\theta} = 15°$ (not shown in the figure). However, under influence of oblique waves the longshore current is forced. Especially in the trough between the outer and inner shore parallel bar V^o is a lot weaker for the low value of θ.

Subsequently a sensitivity test to the factors α_{roll} and n_{bor} is done, since these factors describe the roller dynamics and form the newest extension to the MORFO-model series. The model parameter N_{bor} only appears in the sediment transport formulation. Thus varying this parameter only has a direct effect on the depth integrated sediment concentration C_{di}. Figure 4.11 shows that the value of N_{bor} has a positive effect on the sediment concentration. Putting the parameter to zero implies that the sediment stirring by the turbulent eddies after the rollers is not anymore taken into account, so that the overall stirring is less strong. On the other hand variation of the model parameter α_{roll} has a less easy describable effect, see figure 4.12. The factor α_{roll} determines how much of the dissipated wave energy is transferred to roller energy. When the

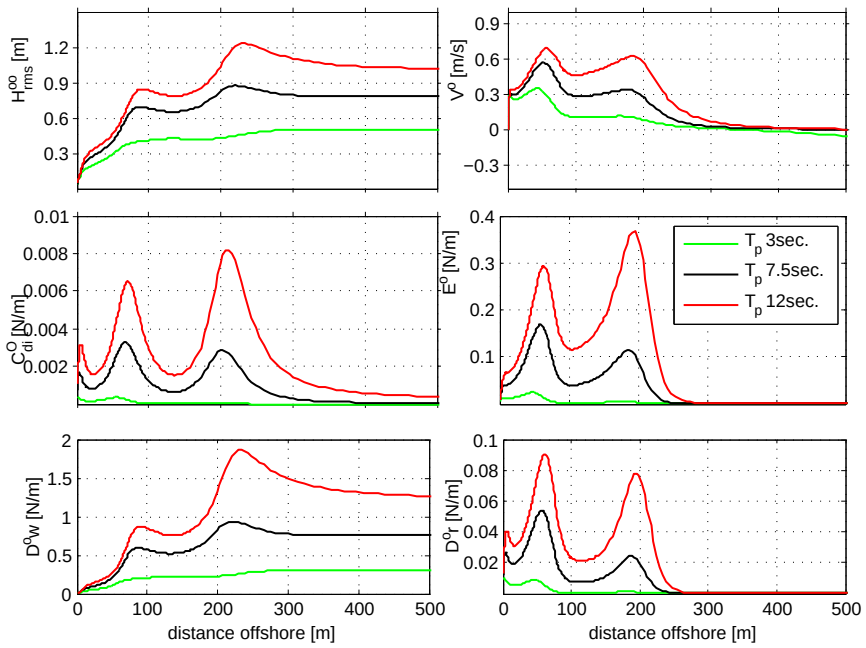

Figure 4.9: As figure 4.8, but then for basic state sensitivity to offshore wave period $\widehat{T}_{peak}$.

factor is lowered or even put to zero, the peak in the longshore current shifts slightly seaward, to exactly above the bar crests, and the value of the peak is higher. When α_{roll} is low, less energy is going into the rollers (this is shown in the third graph plot of figure 4.12, whilst the wave energy density profile is insensitive to this parameter. The reduction in roller energy may be compensated in the increased intensity of the longshore current. Lowering α_{roll} reduces the sediment concentration peak around the inner bar, because the turbulent velocity that stirs up sediments is then lowered too.

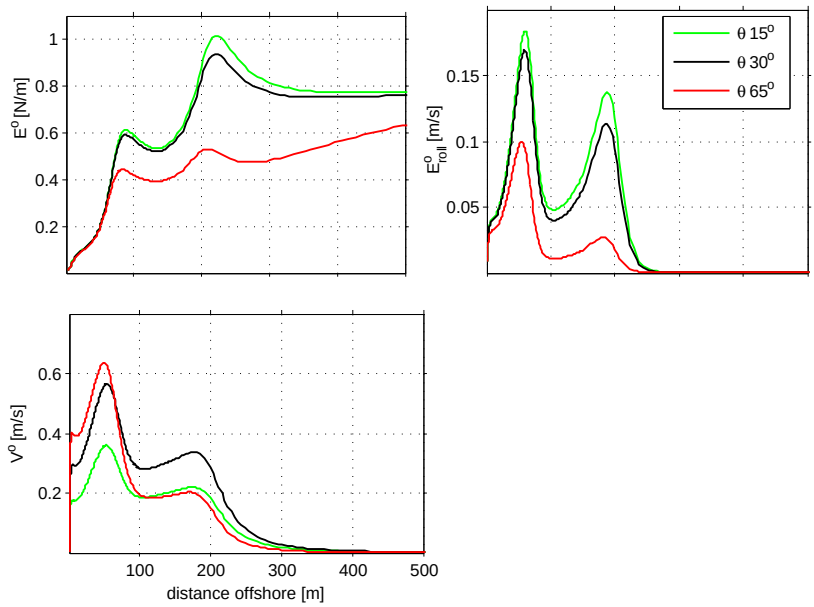

Figure 4.10: As figure 4.8 for basic state sensitivity to offshore wave angle $\widehat{\theta}$. Changing this wave condition shows back on the energy density E^o, roller energy density E^o_{roll} and the longshore current V^o.

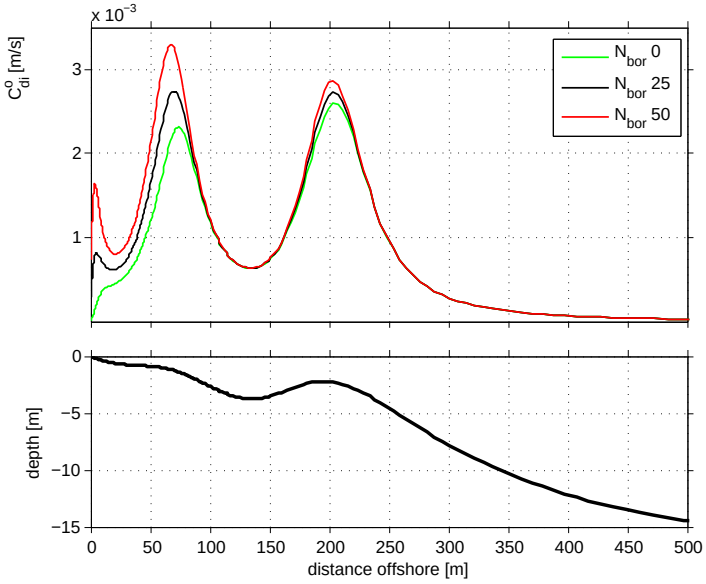

Figure 4.11: Basic state sensitivity to the sediment stirring parameter N_{bor}. By default $N_{bor} = 50$. The upper plot shows the effect of a lower value to the depth integrated sediment concentration C^o_{di}. For clarity the bottom plot, showing the sea floor profile, is added.

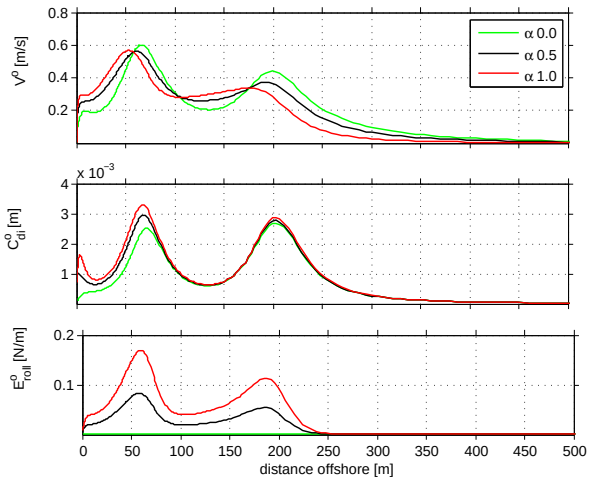

Figure 4.12: Basic state sensitivity to the energy-partition factor α_{roll} on the longshore current V^o, the depth-integrated sediment concentration C^o_{di} and the roller energy density E^o_{roll}.

4.2.3 Linear stability analysis; default case

The next step is the linear stability analysis. The basic state resulting the default setting (see paragraph 4.2.1) is perturbed with a series of perturbations sized the longshore wavenumber κ, where κ is the angular reciprocal of the wave length λ; $\kappa = 2\pi/\lambda$. This reveals the presence of one main solution, one growing mode. Figure 4.13 shows the growth rate Ω for the dominant mode, for each κ in the domain $0.01 \leq \kappa \leq 4.0m^{-1}$. Also the migration rate curve is plotted. Bed form perturbations sized $\kappa[0.068 : 0.332m^{-1}]$ cause an instability and may grow further. The fastest growing mode (FGM) is the perturbation associated with the maximum growth rate, Ω_{max}. For the default case $\Omega_{max} = 0.48h^{-1}$, which corresponds to an e-folding growth time of 5.7 hours. The fastest growing mode has $\kappa_{pref} = 0.216m^{-}1$, hence the modeled dominant perturbation wave length $\lambda_{pref} = 29.0m$. The migration rate of these bars $c_{pref} = 0.194mh^{-1}$.

A visualization of the bars resulting the fastest growing mode perturbation is given in figure 4.14: a rhythmic pattern of very oblique bars and troughs, extending 10 to 15 meters seaward from the alongshore axis. For the default case the waves approach the coast under an offshore wave angle of 30°. Positive wave angles represent waves coming from the South to the East, being from the left in the first topography plot. The waves induce a mean longshore current northwards along the beach, so from left to right. The crests of the sand bars appear to point towards the left, hence they have an up current orientation. The obliqueness of the modeled finger bars seems a bit exaggerated compared to what was observed.

In figure 4.14 also the deviations of the longshore current, induced by the forming bars, are plotted, by means of small black arrows. An offshore current deviation is directed over the bar crests, whilst in the troughs the shoreward component of the current is increased. This indeed is expected to feed back positively to the developing transverse finger bars, as explained in section 2.3. What happens if the offshore wave angle is put negative, representing waves from the northeast? The right topography-plot in 4.14 shows that the same pattern of bars is found, with their bar crests pointing in the opposite direction. So for both positive and negative incoming wave angles up-current bars are found, with about the same characteristic spacing λ_{pref} of 29.8m. and $\Omega_{max} = 0.45h^{-1}$.

The characteristics of the modelled bars, the size, maximum growth rate and migration rate are expected to be dependent on the wave parameters and roller dynamics. This sensitivity to the parameters is presented in the following paragraphs. It is assumed that the results for negative and positive offshore wave angle will be approximately equal, so in all tests only positive values of the model parameter $\widehat{\theta}$ are used.

4.2.4 Linear stability analysis; sensitivity to wave conditions

In section 4.2.2 the basic state turned out to be sensitive to the offshore wave angle $\widehat{\theta}$, in the sense that this parameter affects the amount of wave and roller energy densitiy in the system and thus the intensity of the sediment stirring and the strength of the longshore current. These factors are all of importance in the process of transverse finger bar growth, so it is interesting to do a sensitivity analysis to $\widehat{\theta}$. The offshore wave angle is varied from 1 to 89 degrees. Figure 4.16 shows the $\Omega(\kappa)$ and $c(\kappa)$ graphs for three different values of $\widehat{\theta}$. Below $\widehat{\theta} = 20°$ no initial bar growth is found. There is a clear positive relation between the growth rate and the obliqueness of the incoming waves until a certain limit value of $\widehat{\theta}$. This limit lies approximately at $\widehat{\theta} = 70°$; when the offshore wave angle is even higher the growth rates will in general be less. The same applies for the relation between offshore wave angle an the migration rate. The plots for $\widehat{\theta} = 20, 30$ and $70°$ show that whilst Ω_{max} increases, the dominant wavenumber κ_{pref} decreases, implying that the perturbations alongshore wavelength λ_{pref} is larger. This is visualized in figure 4.15. The

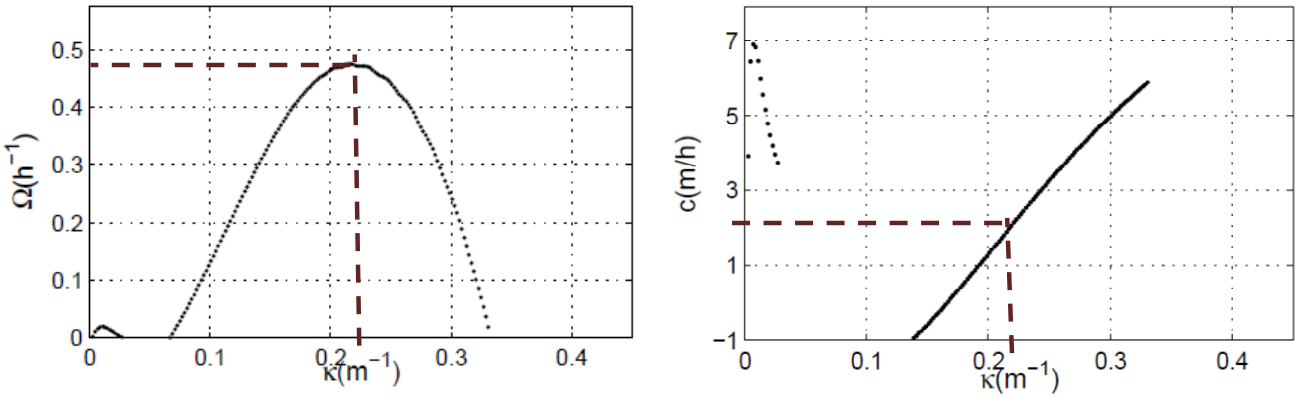

Figure 4.13: Linear stability analysis result for the default setting. Left: curve of the growth rate Ω of the the most dominant mode versus each perturbation wavenumber κ. Right: curve of the migration rate c versus each κ.Vertical red line indicates the fastest growth rate, $\Omega_{max} = 0.48$, resulting a perturbation sized $\lambda_{pref} = 29.0m$ ($\kappa_{pref} = 0.216m^{-1}$), that migrates with $c_{pref} = 1.94m^{h-1}$

obliqueness of the modeled fingerbars is even higher for the higher value of $\widehat{\theta}$.

Comparing this result to what is observed at the Gold Coast, it shows that the lower limit of transverse finger bar growth given by the model about equals the lower limit of the average $\widehat{\theta}$ preceding the observed bar growth. The upper limit of $\widehat{\theta}$ resulting the model however lies $20 - 30°$ higher than what follows from the observation analysis. The wavelength of the bars and their up-current orientation do compare well to what was on average observed at Surfer's Paradise.

Subsequently the sensitivity to the offshore wave height $\widehat{H}_{rms}$ is tested. This seems to be very relevant to do, since varying this parameter, like $\widehat{\theta}$, had a significant effect on the basic state solution of the wave and roller energy density, the intensity of the breaking, the longshore current and thus the sediment concentration. The wave angle is kept constant at a value of $\widehat{\theta} = 30°$, but the wave height is varied from 0.2 to 1.2 meter, this results the $\Omega(\kappa)$ and $c(\kappa)$ curves as shown in figure 4.17, where the curves resulting $\widehat{H}_{rms} = 0.3, 0.4, 0.5, 0.8$(default setting) and$1m$. are plotted. There is a positive relation between the offshore wave height and both the growth and migration rates. $\widehat{H}_{rms} = 0.3$ is a minimum input wave height for the linear stability analysis to result initial bar growth. For $\widehat{H}_{rms} > 1.2$ no model result was obtained. Whether this is simply the limiting height for bar growth, or a numerical inconvenience of the model, is not clear. However, since this value compares well to the upper limit of offshore wave height following the observed transverse finger bars at Gold Coast, this question was left unsolved. From the $\Omega(\kappa)$-graph in figure 4.17 it follows that also here the increase in growth rate, and thus Ω_{max}, for higher incoming waves goes together with a shift to lower values of κ_{pref}, but the differences are small.

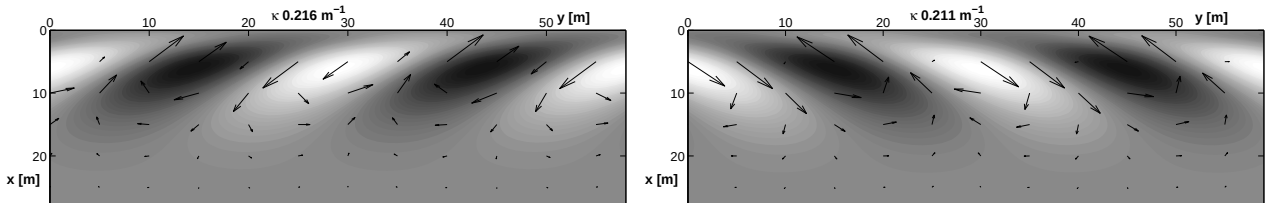

Figure 4.14: Left: topography plot resulting the fastest growing solution of the linear stability analysis to the default case: an alongshore perturbation characterised by $\lambda_{pref} = 29.0m$. Here the x-axis is the cross-shore axis, the y-axis at the top forms the shoreline ($x = 0$); white areas indicate bed elevation (bar crests), darker areas represent troughs; The arrows represent the perturbation of the current velocities, showing offshore flow over the crests, shoreward flow in the troughs. Right: same plot for the default setting with offshore wave incidence angle put to $-30°$ in stead of $30°$ so for waves from the other direction. The bars again are up-current, with an about equal spacing.

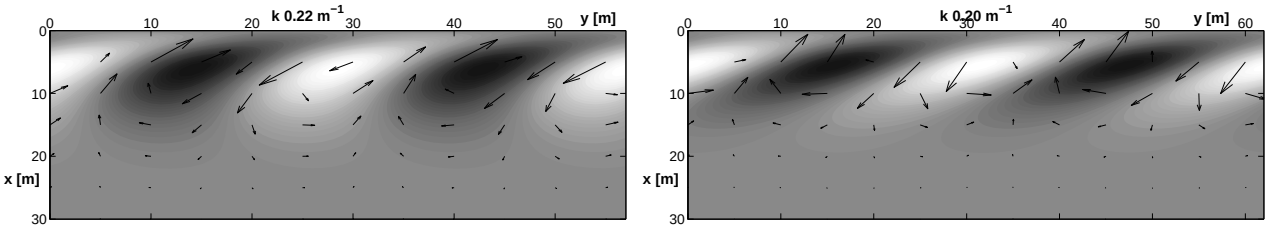

Figure 4.15: As figure 4.14. Here the topographies for the bed perturbation with the largest growth rate when the offshore wave angle, $\widehat{\theta}$, is $20°$ (left) and $70°$ (right). The perturbations are sized $\kappa_{pref} = 0.22$ and $0.20m^{-1}$ respectively ($\lambda_{pref} = 28.5$ and $31.5m$)

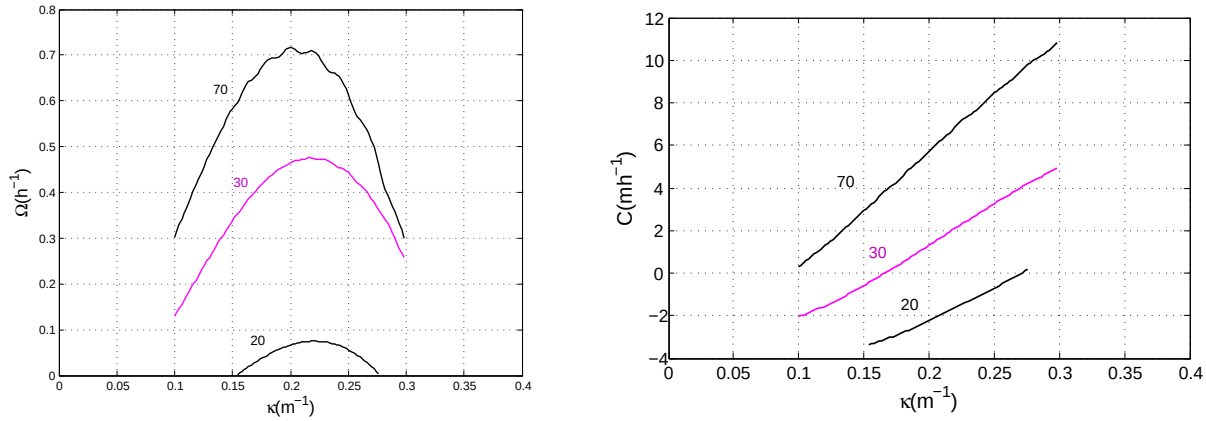

Figure 4.16: Growth rate and migration rate curves resulting different values of the offshore wave angle $\widehat{\theta} = 20^o, 30^o, 70^o$. The rest of the model setup is as the default setup. The curve of $\widehat{\theta} = 30^o$ is drawn in purple, because this is the default setting.

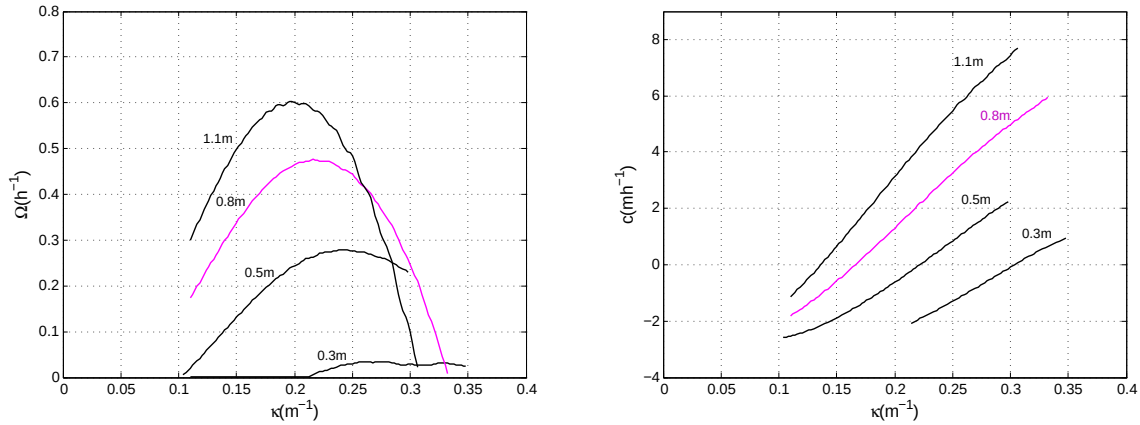

Figure 4.17: As figure 4.16 but here different values of the offshore wave height, $\widehat{H}_{rms}$, are tested. Left the growth rate curve, right the migration curve, for $\widehat{H}_{rms} = 0.3m, 0.5m, 0.8m$ (default setting; in purple) and $1.1m$.

So, both the energy of the incoming waves (proportional to the offshore wave height squared) as the offshore angle of wave incidence $\widehat{\theta}$ influence the growth of nearshore rhythmic bed forms. It would be interesting to study the combined effect of both parameters. The wave height domain $\widehat{H}_{rms}[0.2:1.2]$ turned out to result in growing modes, for a value of $\widehat{\theta}$ of 30°, as did the wave angle domain $\widehat{\theta}[20:85]$ for $\widehat{H}_{rms} = 0.8$. But does each combination of $\widehat{\theta}$ and $\widehat{H}_{rms}$ of these domains result in transverse finger bar growth? To answer this question, the model is run with each of the combinations of wave parameters from the following domains: $\widehat{\theta}: 20, 25, 30, ...85°$ and $\widehat{H}_{rms}: 0.2, 0.3, ...1.2m$.. Figure 4.18 is the first result from this test. It shows the $\Omega_{max}(\theta)$-curves; the largest growth rate obtained for each $\widehat{\theta}$ for different values of $\widehat{H}_{rms}$. For the higher waves the results scatter a bit, but a positive relation between the maximum growth rate and the offshore wave angle of incidence can be discerned, up to a certain optimum $\widehat{\theta}$. Setting wave angles above this optimum results in lower values of Ω_{max} again. Also it shows that, the lower the offshore wave height, the narrower the range of wave angles for which a growing mode is found.

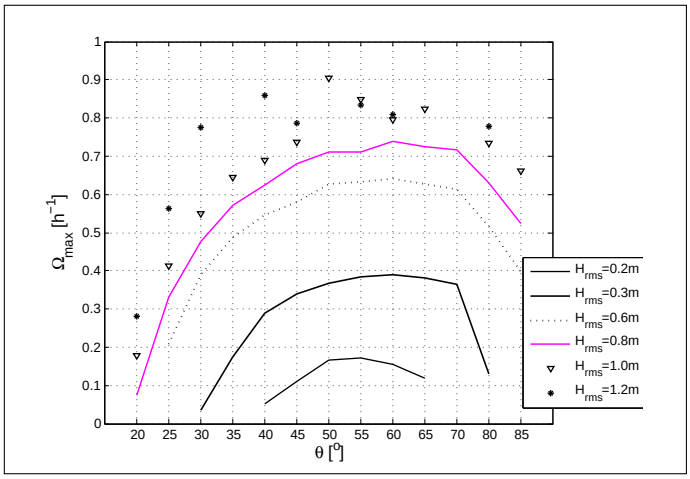

Figure 4.18: Curves of the maximum growth rate Ω_{max} versus $\widehat{\theta}$ for different values of the offshore wave height $\widehat{H}_{rms}$

By means of a contour plot this is illustrated again in figure 4.19. When the offshore wave height is 0.7meter or larger, waves with an offshore angle from the whole range of $\widehat{\theta}[20:85°]$ will result in transverse finger bar growth. For lower waves, the wave angle range resulting bars becomes narrower, being only 40 to 65° when $\widehat{H}_{rms}$ is reduced to 0.2.

The plots in figure 4.20 show more or less the same behavior in the relation between the migration rate C and the wave angle, for the different values of $\widehat{H}_{rms}$. The optimum value of κ, the perturbation wave number for which the highest growth rates are found is negatively related to the wave height and the wave angle. It is hard to determine the optimal conditions for the growth of transverse fingerbars from these results. It seems that higher wave angles favour the growth, but an H_{rms} of 1.2 meter is the limit height the model could coop with.

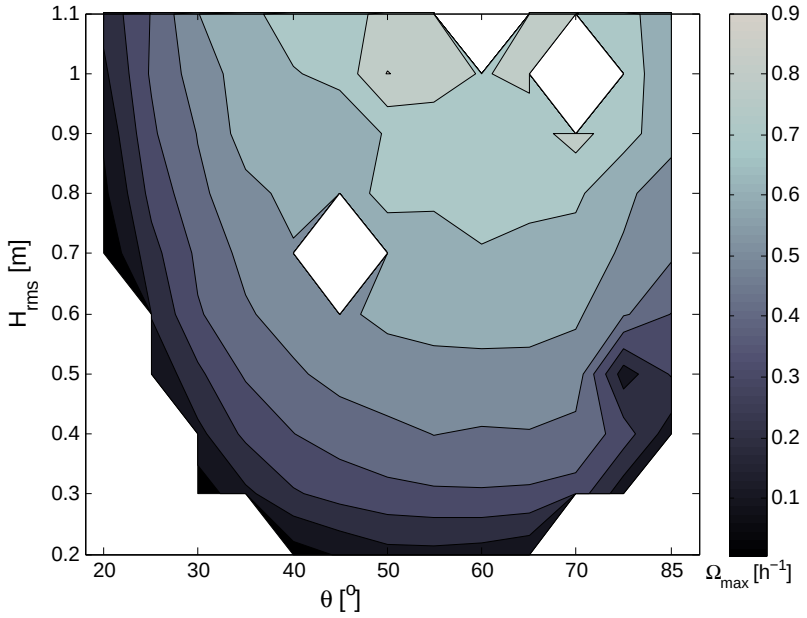

Figure 4.19: Contour plot of the maximum growth rate Ω_{max}. On the y-axis the variable offshore wave height H_{rms}, on the x-axis the offshore wave angle θ. The white areas in the plot indicate that these combinations of $\widehat{H}_{rms}$ and $\widehat{\theta}$ gave no result.

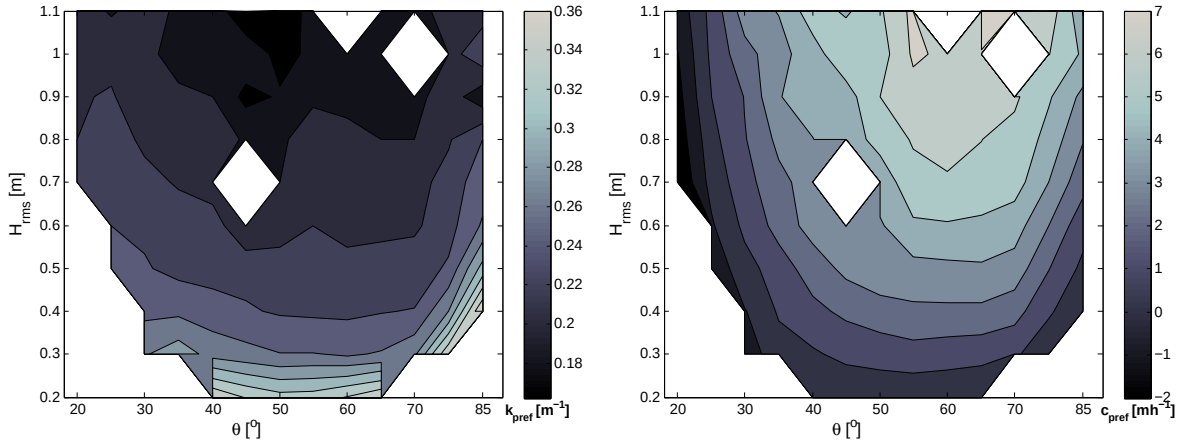

Figure 4.20: Contour plots of the perturbation wave number (left) associated with the maximum growth rate, κ_{pref}, and the associated migration rate c_{pref} (right), showing their sensitivity to the offshore wave height (on the y-axis) and the offshore wave angle (x-axis). White areas indicate that for these combinations of $\widehat{H}_{rms}$ and $\widehat{\theta}$ the model gave no result

4.2.5 Sensitivity to model parameters: α_{roll} and N_{bor}

First a note must be made on the model implementation with respect to the roller dynamics. The roller radiation stresses can be excluded from the momentum balance (equation (3.2)), thus implying that all roller-related terms in the model are ignored. This can be done for the basic state determination and the linear stability analysis separately. In the study to Noordwijk beach it was seen that turning the rollers off in the LSA led to a different model result (personal communication C. Ribas). Here however, it turned out that when including the perturbations of the roller dynamics in the stability analysis, no stable solution would be found. Previous LSA results are all obtained without including the roller perturbations in the model. This is further discussed in appendix C

However it is essential to include the roller dynamics in the basic state calculation. In this paragraph the sensitivity to the model parameters, α_{roll} and N_{bor} , is presented. These parameters are related to the rollers, and thus do not influence the linear stability analysis directly, but the LSA result is still sensitive to their effect in the basic state determination. The factor α_{roll} requires to be at least put to 0.5 (it is set to 1.0 in the default model setting) for the LSA to give any result at all. Figure 4.21 shows the growth rate and migration rate graphs where α_{roll} has been varied from 0.5 to 1.0. The higher the amount of broken wave energy dissipation transferred to the roller, the easier and quicker bars will be growing in the nearshore zone. The distance between the bars is slightly higher too as is the migration rate, for higher α_{roll}.

But, some simple try-out runs showed that also for lower values of α_{roll} transverse finger bar growth could occur, provided the offshore wave angle $\widehat{\theta}$ was higher than 50°. Consequently a series of sensitivity tests to the effect of co-varying α_{roll} and $\widehat{\theta}$ is done. The result is summarized in figure 4.22. This contour plot shows the maximum growth rates for all combinations of $\alpha_{roll}[0.1, 0.2...1.0]$ and $\widehat{\theta}[20, 30...70°]$. Low values of α in combination with an offshore wave angle of 60° or more do can result in transverse finger bar growth, according to the model. However, growth rates are relatively low in these cases; Ω_{max} on the order of $0.1h^{-1}$ corresponds to bar growth times of about 27 hours. Highest maximum growth rates result the combination of a large $\widehat{\theta}$ and high values of α_{roll}.

Finally, also the factor N_{bor} promotes the growth of transverse finger bars, as can be seen in figure 4.23, the result for model runs with N_{bor} put to 25, 35, 50 (default setting) and 60). Increase of N_{bor} promotes the stirring of sediment by the rollers of the broken waves, so that more sands for bar growth are provided. This shows back in higher growth rates. Remarkably here these higher growth rates do not come together with a larger space between the bars (hence a lower κ at the peak value of ω) like in the other sensitivity tests. It even seems that the optimum κ shifts slightly to higher values when N_{bor} and ω_{max} increase. Another thing that catches the eye are the migration curves, in the right plot of figure 4.23: until $\kappa = 0.225m^{-1}$, ($\lambda = 28m$) the migration rate is negatively correlated to N_{bor}, after that the relation is positive.

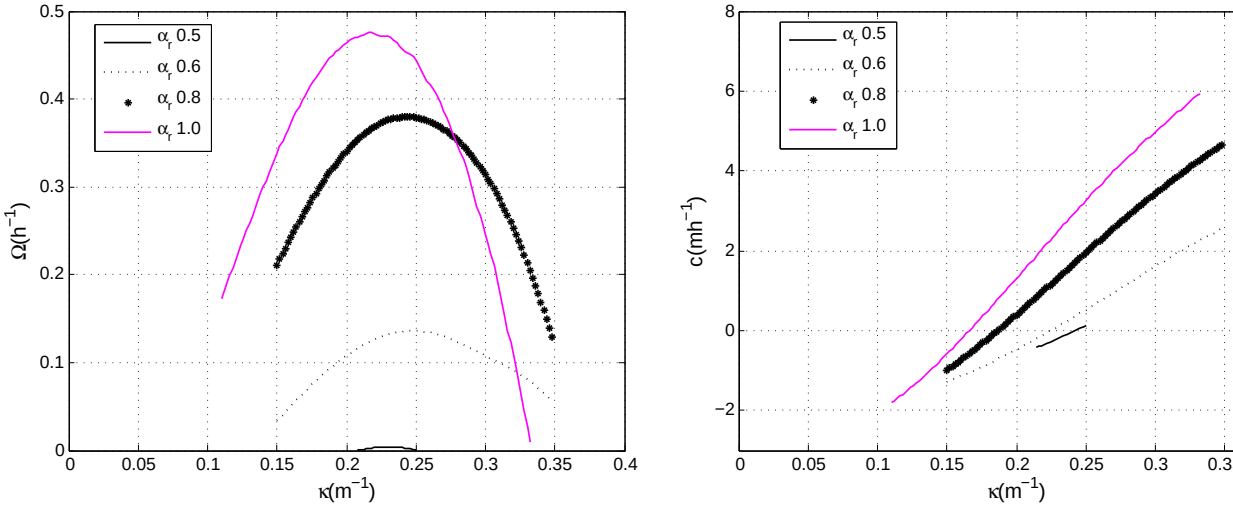

Figure 4.21: Growth-rate curves (left) and migration rate curves (right) for the default model setting with $\alpha_{roll} = 0.5, 0.6, 0.8$ and 1.0 (default: in purple)

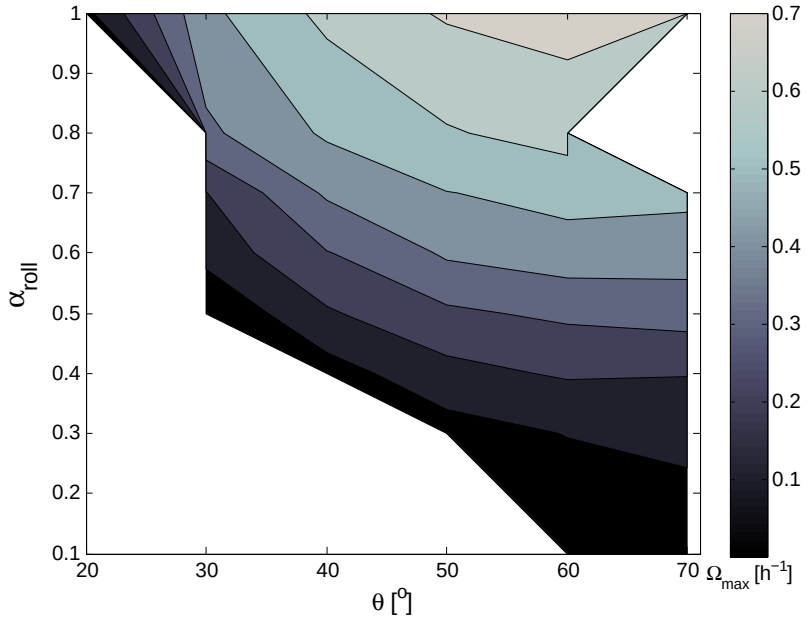

Figure 4.22: Contour plot of the maximum growth rate Ω_{max} for each of the combinations of energy partition factor, $\alpha_{roll}[0.1 : 1.0]$ (y-axis), and offshore wave angle $\theta[20 : 70°$ (x-axis).

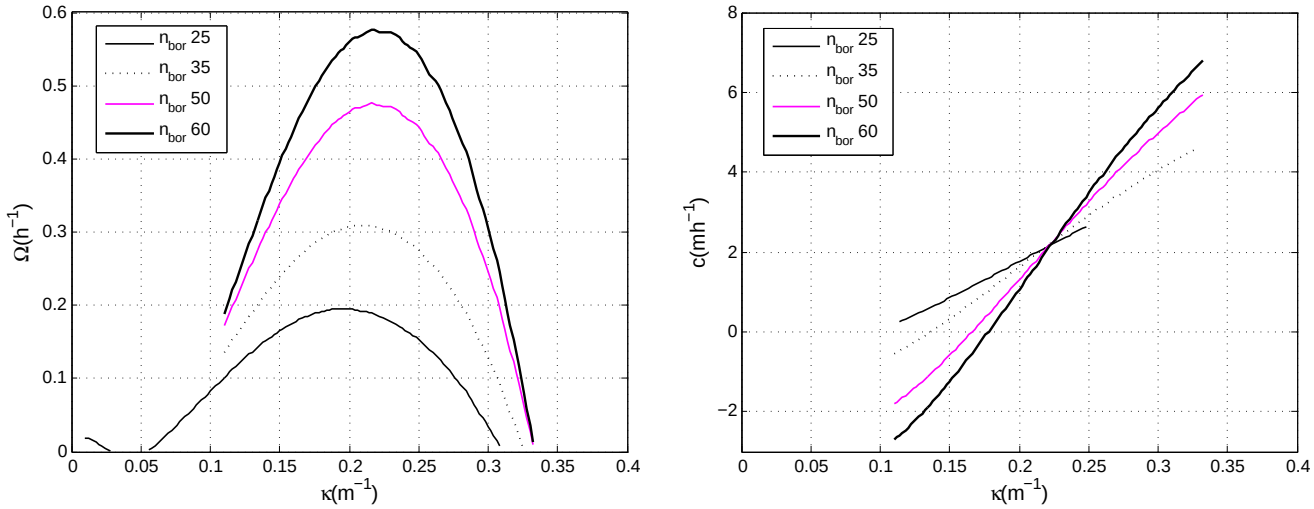

Figure 4.23: as figure 4.21 for $N_{bor} = 25, 30, 50$ (default setting; in purple), and 60. Left the growth rate curves, right the migration rate curves

4.3 Interpretation of the model results

To summarize the results it is convenient to repeat the hypotheses and the theory on transverse finger bar growth, as described in section 2.3. Transverse finger bars growth is expected to be influenced by the amount of energy the waves contain and the incoming wave angle. Next to that, the turbulent rollers that develop when waves break would be important. According to the theory, it is the longshore current deflection over the bars due to both mass conservation (Trowbridge) and frictional torques, that positively feeds back to initial growth of up-current transverse finger bars. From the sensitivity analysis of the basic state it shows that the intensity of the longshore current is positively related to the offshore wave height $\widehat{H}_{rms}$. There is also a positive relation between the longshore current and the offshore wave angle, but only up to an optimum value of $\widehat{\theta} = 70°$. The result of the linear stability analysis shows that for $\widehat{\theta} < 20°$ and $\widehat{H}_{rms} < 0.2m$. no bars grow, and that the maximum growth rate increases with increasing wave height and with increasing wave angle up to a certain optimum at $55° < \widehat{\theta} < 70°$. This optimum $\widehat{\theta}$ follows from the fact that very oblique incident waves have a lower wave height when arriving at the surf zone. This makes that the wave energy and thus the breaking is slightly reduced.

Rollers are said to have both a positive and a negative feedback on transverse finger bar growth, via the alongshore respectively the cross-shore component of the radiation stresses they invoke. From the basic state sensitivity analysis it turns out that both the offshore wave height and wave angle positively affect the roller energy density and thus the strength of the roller radiation stresses via the roller energy density (note: $\widehat{\theta}$ optimum value of 65° again). The alongshore roller radiation stresses are proportional to $\sin 2\theta$, whereas the cross shore component is proportional to $\cos\theta \sin\theta$ (see equation (3.7)), thus for smaller θ the dampening cross-shore component S^r_{xx} will probably dominate. This may explain why in the linear stability analysis for $\widehat{\theta}$ no growing modes are found.

The importance of the rollers follows from the LSA to the model's sensitivity to the combined effect of α_{roll} and $\widehat{\theta}$. From figure 4.22 can be concluded that, when waves approach the surf zone under an intermediate angle ($\widehat{\theta} = 20 - 40°$), at least half of the wave energy should go into the rollers for growing modes to result the LSA. However, very obliquely incoming waves will make the model predict transverse finger bar growth for very low values of α_{roll}, so even when rollers are not so intense. Apparently the Trowbridge mechanism is then strong enough. Turning the rollers off completely is not desirable. The general reduction of Ω_{max} when offshore wave angle exceeds 70° must be caused by the reduction of the longshore current.

5 Discussion

A four years data-set of Argus time-exposure images showed that transverse finger bars are a regularly occurring phenomena in the nearshore of Surfer's Paradise beach, on the Gold Coast of Australia. The 10-minute averaged images are a useful means to determine the zones of preferential wave breaking, indicating the location of submerged alongshore and cross-shore sand bars. With this method the occurrence and characteristics of the transverse finger bars can be studied for a longer period of time.
Each observation of 3 or more transverse finger bars in a patch, visible for two or more days, is called a transverse finger bar event. For each event the typical wave length (inter-bar spacing) and orientation of the finger bars could be determined. Next to these characteristics the duration and number of bars per event are documented. Transverse finger bar presence at Gold Coast is 24% of the time, with an average wave length of 32m. The bars are most often seen to have an up-current orientation. Earlier observations of up-current orientated transverse finger bars have been done at Duck beach (Ribas *et al.* (2011a)) and Noordwijk beach (Ribas & Kroon (2007)). The Gold Coast differs from these coasts in the sense that the offshore slope is a lot steeper. At Surfer's Paradise beach the transverse finger bar occurrence is generally higher than in Duck and Noordwijk. However, the wavelength of the Gold Coast finger bars and the fact that they are only attached to the inner alongshore bar, compares well to the Noordwijk finger bar characteristics.

Hourly information about the wave height H_{rms}, wave period T_{peak} and wave incidence angle θ at 18m. water depth, permits the determination of the offshore wave conditions before and during each transverse finger bar event. As expected, transverse finger bars are typically related to intermediate wave conditions: $\widehat{H}_{rms} = 0.7$ m, $\widehat{T}_{peak} = 9.2$ sec. and $\widehat{\theta} = 28°$, which are about the annual average wave conditions at the Gold Coast. These average annual wave conditions lie close to the average annual wave conditions at Noordwijk beach.

However, the offshore wave angle record is a bit doubtful. The event-preceding wave range is wider than expected. Especially the lower limit of $\widehat{\theta} = 0°$ (normally incident waves) is strangely low. Since the wave angle is not recorded by the Gold Coast wave rider buoy itself, but by a more distant buoy, this may explain the inconvenience. It can also be that due to the nearshore morphology the waves are thus changed that the offshore incoming wave angle isn't a useful measure to characterise the flow pattern in the surf zone any more. This makes it also hard to state whether the observed bars are truly up-current or not. It is not investigated specifically how constant the incoming wave angle and the other offshore wave conditions were, before a transverse finger bar event was observed and during the event. This may be of influence to the finger bar characteristics as well, a subject to study a little further in the future.

In the analysis of the transverse finger bar characteristics of Surfer's Paradise beach, few attention has been paid to the migration rates. The reason for this is that unfortunately the

observed bars seemed not to migrate clearly, and there were to few events with a long enough duration to do a trustful quantitative analysis to the bar migration.

A limiting thing of using Argus time-exposure images in the analysis of transverse finger bars is that the bed relief needs to have a certain size before it is discernable on the images. This means that the moment finger bars are first observed, called the starting point of an event, is in reality not the starting point of the bar formation. This makes it hard to determine the exact growth rate of an initial bar-like bed perturbation. One can only conclude the growth rate to be of the order of one day. Also the determination of the event-preceding wave conditions is therefor a bit less effective.

The nearshore morphology can be described by means of the state of the alongshore parallel bars, as done by Price & Ruessink (2011). The question is whether, apart from the wave conditions, also this bar state influences transverse finger bar growth? In the nearshore zone of Surfer's Paradise beach, in general an outer (more seaward) bar and an inner bar can be discerned. Following the classification by Price & Ruessink (2011) shows that in 50% of the transverse finger bar events the inner bar was in an rLTT -state (rhythmic low tide terrace), where the bar is semi-attached to the shoreline, whilst the outer bar had a TBR-morphology (transverse bar and rip), a strongly undulating bar with shoreward pointing transverse protrusions. However, from this analysis one cannot be really sure whether the alongshore bar state is of influence to finger bar formation. The bar states seen mostly during transverse finger bar events are, like the finger bars, typical of low to intermediate energy conditions.
It do is remarkable that the fingerbars were mainly seen to grow on the straighter parts of the shoreline, where there was still a (semi-) continuous trough between the inner and outer bar. Ribas & Kroon (2007) also found a minimum value of spacing between the inner and outer bar required for transverse finger bar growth. This requirement is probably due to the longshore current: deflection of this current is the main physical mechanism behind transverse bar formation, so for the mechanism to work the longshore current should have some space to flow freely. It is mainly the outer shore parallel bar that determines the hydrodynamics in the trough.

The morphodynamic model MORFO62 performed quite well in reproducing the Gold Coast transverse finger bars, after the appropriate numerical calculation grid was defined. The cross-shore topography profile was a highly simplified version of the 2002 bathymetric survey at Surfer's Paradise beach, consisting of two thresholds formed by the two alongshore bars, followed by a relative steep slope to an offshore depth of 18m. The default wave parameter setting, representing waves with properties that lie close to the average finger bar event-typical properties deduced from the observations, results the initial growth of up-current orientated transverse finger bars with a growth rate of $0.48h^{-1}$, a migration rate of 0.194 mh^{-1} and a typical wave length of 29m. This λ corresponds very well to observations. Whether the growth rate and migration rate predicted by the model are realistic or a bit exaggerated is hard to say, since these cannot be determined exactly from the Argus-images. An Ω_{max} of $0.48h^{-1}$ corresponds to a growth time of 6 hours, which falls nicely within the limit of one day. Intuitively also the predicted migration rates have the right order of magnitude. Where in former studies (Ribas *et al.* (2011b);Ribas *et al.* (2011a)) in general too high values were found for the migration rates of the fastest growing mode, this doesn't seem to be the case here.

Looking to the basic state equilibrium, it shows that wave breaking takes place over the alongshore bars, by which turbulent rollers are formed and the longshore current is forced. Sensitivity analysis shows that these processes are positively influenced by the height of the offshore incoming waves, certainly up to a $\widehat{H}_{rms}$ of 1.2 m. and a wave incidence angle of $\widehat{\theta} = 70°$. The linear stability analysis then indeed shows that initial growth of transverse finger bars takes place

for $\widehat{H}_{rms}$ ranging from 0.2 to 1.2 meter, and for $\widehat{\theta}$ between 20° and 85°, with highest growth rates for the highest waves and $\widehat{\theta}$ of 70°. Especially the modelled wave height range compares very well to the observed range.

Comparing the model results for the Gold Coast with what was said about the hydrodynamic mechanisms involved in transverse finger bar growth, by Ribas *et al.* (2012), gives a good insight. As explained in section 2.3, two mechanisms involving the longshore current are promoting transverse finger bar growth, whilst the turbulent rollers partly promote and dampen the process. The mechanism first described by Trowbridge (1995) relates bar growth to the offshore deflection of the longshore current. For this mechanism, the longshore current needs to be of a certain intensity. The wave incidence angle and the wave height both positively influence the longshore current intensity, which is a first explanation why there is a minimum $\widehat{H}_{rms}$ and $\widehat{\theta}$ required. The effect of the frictional torques was not studied here. The longshore current deflection should go together with a depth integrated sediment concentration that decreases in offshore direction. The effect of the roller dynamics in the model would be twofold: the longshore component of the roller radiation stresses ($\sim sin\theta$) is said to promote bar growth, whilst the cross-shore component would dampen finger bar growth. However, as described in 4.2.5 and illustrated in appendix C, the roller dynamics are not taken into account in the linear stability analysis. They do are necessary to include in the basic state calculation. The roller parameters α_{roll} and N_{bor} influence the equilibrium energy balance, sediment distribution and sediment availability. When α_{roll} and N_{bor} are too low, apparently too few sediment is available for finger bar growth.

Although the performance of the model is not bad at all, a linear model like MORFO62, which assumes an initially uniform bed profile in the alongshore direction may not be adequate enough to correctly model the Gold Coast transverse finger bars. From the observations it seems that the finger bar occurrence is related to the overall nearshore morphology. The alongshore bar states preferentially occurring when finger bars are present, have a typical alongshore variability. Using a non-linear model, that can interpret alongshore variation in the initial topography, may be interesting in a future research project to better discern which processes dominate transverse finger bar formation.

6 Conclusions

In this project transverse finger bars in the surf zone of Surfer's Paradise beach on the Gold Coast, East Australia, have been investigated, by means of the analysis of time-exposure image observations (ARGUS) and an existing morphodynamic model based on linear stability analysis, MORFO62 (Ribas *et al.* (2011b)). Argus-images taken at the daily low tide hours from November 1999 to October 2003 are analysed. It is concluded that transverse finger bars are a regularly occurring phenomena on the Gold Coast beach, the bars being present on 24% of the days, arranged over a total of 69 events. The size of the events was quite variable: The duration of an event varied from 2 to a maximum of 21 days. The average number of bars in a patch was 6, however the range was from 3 to 15 bars per event. The transverse finger bars appeared within a day, and did not significantly seem to move along the shoreline. The inter-bar spacing, the wavelength λ, ranged from 17 to 71 m. , with an average of 32 m.

Information about the offshore H_{rms}, wave period T_p and wave incidence angle θ from two wave buoys is used to study the relation between transverse finger bar occurrence and offshore wave conditions. For each event the 24h- average offshore wave conditions are determined. This results in the following average pre-event wave conditions: an event average offshore wave height of 0.7 m., an offshore average peak period of 9.2 sec. and an offshore average incoming wave angle of 28° are determined. These values lie very close to the multi-year average wave conditions recorded at the Gold Coast. The range of the offshore wave height related to transverse finger bar occurrence is extends from 0.3 to 1.2 m., the offshore wave period, $\widehat{T_p}$, ranges from 5.8 to 14.4. Ranges and averages correspond to waves of an intermediate energy level, following expectations. It was also expected that the finger bars would result waves with an oblique incidence angle with respect to the shore normal. The absolute value of the average offshore wave angle preceding the transverse finger bar events ranged from 0 to 85°, which is an unexpectedly large range.

The majority of the time the waves approach the coast from the Southeast. The observed transverse finger bars were most often orientated with their crests pointing in southeastern direction, so in general up-current bars seem to be formed. Only in 27% of the time a northeastern finger bar orientation was observed. Whether these are also up-current does not follow clearly from the recorded offshore wave incidence angle. It seems that the offshore wave angle $\widehat{\theta}$, is not certainly explaining the finger bar formation and orientation.

The nearshore morphology of Surfer's Paradise beach is characterised by two alongshore parallel bars, with a variable shape. The bars are characterised by the bar state classification of Price & Ruessink (2011). Following this classification, it shows that transverse finger bars develop only when the shore parallel bars are in a state that represents lower energy (reflective side of the bar-state sequence). In 50% of the cases transverse finger bars are seen, when the inner (shoreward) bar was in an rLTT -state (rhythmic low tide terrace), whilst the outer bar was in TBR-state (transverse bar and rip), a strongly undulating bar with shoreward pointing transverse protrusions.

The model MORFO62 first determines a basic state, the equilibrium balance between waves, longshore current, sediment transport and the sea bed. Hereupon a linear stability analysis (LSA) to a series of sea bed perturbations is effectuated. The model proved succesful in predicting the initial growth of transverse finger bars for a default case wave parameter setting, that represents waves with properties that lie close to the average event-typical properties deduced from the observations. For this setting bars with an up-current orientation are predicted, with an inter-bar spacing λ of 29 m., which is in close correspondance to the observed average wave length. For the default case a growth rate of $0.48h^{-1}$ (e-folding growth time of 6 hours) and a migration rate of 0.194 mh^{-1} are predicted, which both are very realistic too.

Sensitivity analysis to the offshore wave conditions shows that in the basic state the height of the incoming waves positively influences the strength of the equilibrium longshore current V^o and the intensity of the wave breaking, E^o_{roll}. Regarding the offshore wave angle there is a positive relation between this $\widehat{\theta}$ and the longshore current V^o and a negative relation between $\widehat{\theta}$ and E^o_{roll}. This shows back in the sensitivity analysis of the LSA: maximum growth rates of the initial bars are higher for higher incoming waves, and also for larger offshore wave incidence angle $\widehat{\theta}$, up to a value of $\widehat{\theta} = 70°$. The sensitivity analysis to the wave conditions regarding the LSA shows that initial growth of transverse finger bars takes place when the offshore wave height is ranging from 0.2 to 1.2 meter, and for offshore wave angles from 20° to 85°. The model always predicts up-current bars, with a spacing ranging from 17 to 37 meter.

The turbulent rollers that develop when waves break on the shore parallel bars, induce an extra sediment stirring and a depth averaged sediment concentration-gradient that is negative in seaward direction. This is required for transverse finger bars to grow. According to the model result, rollers are not further promoting the growth of transverse finger bar growth. Here the longshore current is the most determining factor.

Bibliography

Almar, R., Castelle, B., Ruessink, B.G., Sénéchal, N., Bonneton, P., & Marieu, V. 2010. Two- and three-dimensional double-sandbar system behaviour under intense wave forcing and a mesomacro tidal range. *Continental Shelf Research*, **30**, 781792.

Calvete, D., Dodd, N., Falqués, A., & van Leeuwen, S. M. 2005. Morphological Development of Rip Channel Systems: Normal and Near Normal Wave Incidence. *J. Geophys. Res.*, **110**(C10006).

Feddersen, F., Guza, R. T., Elgar, S., & Herbers, T. H. C. 2000. Velocity moments in alongshore bottom stress parameterizations. *J. Geophys. Res.*, **105**(C4), 8673–8686.

Konicki, K. M., & Holman, R. A. 2000. The statistics and kinematics of transverse bars on an open coast. *Mar. Geol.*, **169**, 69–101.

Longuet-Higgins, M. S., & Stewart, R. W. 1964. Radiation stresses in water waves: a physical discussion with applications. *Deep Sea Res.*, **11**, 529–562.

Mohoupt, J., Cee, A.B., Eee, D., & Geehaa., F. 2004. *Wave data recording program. Queensland wave climate annual summary for season 2000-01.* Queensland Government, Environmental Protection AgencyChapman.

Niederoda, A. W., & Tanner, W. F. 1970. Preliminary study on transverse bars. *Mar. Geol.*, **9**, 41–62.

Price, T. D., & Ruessink, B.G. 2011. State dynamics of a double sandbar system. *Cont. Shelf Res.*, **31**, 659–674.

Reniers, A. J. H. M., Roelvink, J. A., & Thornton, E. B. 2004. Morphodynamic modeling of an embayed beach under wave group forcing. *J. Geophys. Res.*, **109**(C01030).

Ribas, F., & Kroon, A. 2007. Characteristics and dynamics of surfzone transverse finger bars. *J. Geophys. Res.*, **112**(F03028). doi:10.1029/2006JF000685.

Ribas, F., Falqués, A., & Montoto, A. 2003. Nearshore oblique sand bars. *J. Geophys. Res.*, **108**(C43119).

Ribas, F., de Swart, H.E., Calvete, D., & Falqués, A. 2011a. Modeling the formation of transverse sand bars: application to Duck beach, USA. *River, Coastal and Estuarine Morphodynamics, bulletin.*

Ribas, F., de Swart, H.E., Calvete, D., & Falqués, A. 2011b. Modeling waves, currents and sandbars on natural beaches: The effect of surface rollers. *J. Marine Syst.*, **88**, 90–101.

Ribas, F., de Swart, H.E., Calvete, D., & Falqués, A. 2012. Modeling and analyzing observed transverse sand bars in the surf zone. *J. Geophys. Res.*, **117**(F02013).

Ruessink, B. G., Miles, J. R., Feddersen, F., Guza, R. T., & Elgar, S. 2001. Modeling the alongshore current on barred beaches. *J. Geophys. Res.*, **106**(C10), 22451–22463.

Ruessink, B. G., L.Pape, & Turner, I.L. 2009. Daily to interannual cross-shore sandbar migration: Observations from a multiple sandbar system. *Cont. Shelf Res.*, **29**, 1663–1677.

Short, A. D. 1999. *Handbook of Beach and Shoreface Morphodynamics.* Chichester: Wiley.

Short, A. D., & Aagaard, T. 1993. Single and multi-bar beach change models. *J. Coastal Res.*, **Special Issue**(15), 141–157.

Soulsby, R. L. 1997. *Dynamics of Marine Sands.* London, U.K.: Thomas Telford.

Splinter, K.D., Strauss, D.R., & R.B.Tomlinson. 2011. Assessment of post-storm recovery of beaches using video imaging techniques: a case study at Gold Coast, Australia. *IEEE Transactions on Geoscience and Remote Sensing*, **49**(12), 4704–4716.

Svendsen, I. A. 2006. *Introduction to Nearshore Hydrodynamics,*. Singapore: World Scientific.

Thornton, B., & Guza, R. T. 1983. Transformation of wave height distribution. *J. Geophys. Res.*, **88**(10), 5925–5938.

Trowbridge, J. H. 1995. A mechanism for the formation and maintenance of shore-oblique sand ridges on storm-dominated shelves. *J. Geophys. Res.*, **100**(C8), 16071–16086.

Turner, I. L., Aarninkhof, S.G.J., Dronkers, T.D.T., & Grath, J.Mc. 2004. CZM Applications or Argus Coastal Imaging at the Gold Coast, Australia. *J. Coastal Res.*, **20**(3), 739–752.

Wright, L. D., & Short, A. D. 1984. Morphodynamic variability of surf zones and beaches: A synthesis. *Mar. Geol.*, **56**, 93–118.

Wright, L. D., Chappell, J., Thom, B. G., Bradshaw, M. P., & Cowell, P. J. 1979. Morphodynamics of reflective and dissipative beach and inshore systems, Southeastern Australia. *Mar. Geol.*, **32**, 105–140.

Zimmerman, J. T. F. 1981. Dynamics, diffusion and geomorphological significance of tidal residual eddies. *Nature*, **290**, 549–555.

A. Transverse finger bar events

On the following two pages the reader can find an overview about the transverse finger bar events recognized in the ARGUS video images series, from 1 November 1999 until 31 October 2003. In total 70 transverse finger bar events were detected and described over this period. As explained in 4.1.1 an 'event' is when at least three bars are visible on the ARGUS images for at least two consequent days. A further classification in the events is made, defining three classes based on the number of bars per patch and the duration of the event, as represented in table 1

Table 1: Classes defined for event classification, based on the number of bars in a patch and the number of consequent days the event was visible on the images. 1-events are called 'developed events', 2-events are called 'well-developed events'

Class	nr. of bars	duration [days]
0	3	2
1	≥ 4	2
1	3	≥ 3
2	≥ 4	≥ 3

The list of events shows the following information about the transverse finger bar events:

- Column 1-4: Start moment of the event; Year-Month-Day-Hour
- Column 5: Event duration [days]
- Column 6: Number of bars
- Column 7: Class of the event (0 or 1 or 2)
- Column 8: Orientation of bar crest with respect to the shore normal; 'N' = towards the north east, 'S' = towards the south east
- Column 9: average wavelength of the bars (inter-bar spacing)
- Column 10: Bar state outer bar
- Column 11: Bar state inner bar. Bar state codes: D: dissipative, LBT: longshore bar and trough, TBR: transverse bar and rip, $eTBR$: erosive TBR RBB: rhythmic bar and beach, LTT: low tide terrace, $rLTT$: rhythmic LTT, R: reflective
- Column12: 24h average offshore wave angle $\widehat{\theta}$ before event start
- Column 13: 24h average offshore wave height $\widehat{H}_{rms}$ before event start
- Column 14: 24h average offshore wave period $\widehat{T}_{peak}$ before event start

e event start				duration	nr.	class	orient-	λ	bar states		pre-event wave conditions: 24h-averages		
year	*month*	*day*	*hour*	*days*			ation	*m*	*outer*	*inner*	θ [°]	*Hrms [m]*	*Tpeak [s]*
1999	12	21	3	5	5	2	S	24	RBB	rLTT	27,0	1,06	7,84
2000	2	18	2	9	4	1	S	-	RBB	LTT	-	-	-
2000	2	22	4	5	5	1	S	27	RBB	LTT	-	0,75	6,00
2000	3	6	4	3	7	1	N	-	TBR	rLTT	5,2	0,90	7,71
2000	3	14	23	3	12	2	S	65,5	TBR	rLTT	19,0	1,01	13,02
2000	3	26	7	3	5	2	S	31	TBR	rLTT	27,3	1,14	8,81
2000	3	28	1	3	8	1	S	-	TBR	TBR	12,9	1,07	8,73
2000	4	13	0	3	4	1	S	27	TBR	TBR	15,1	1,05	8,78
2000	4	19	2	6	3	2	S	23	TBR	TBR	25,8	0,52	9,36
2000	4	22	5	4	3	1	S	24	TBR	TBR	11,5	0,66	11,84
2000	7	11	0	15	3	2	S	29	RBB	LTT	12,7	0,62	11,72
2000	8	13	0	5	5	1	S	28	RBB	R	37,4	0,74	13,06
2000	10	5	1	10	12	2	N	31	RBB	R	42,4	0,56	10,95
2000	10	6	22	4	6	2	N	27	RBB	R	-10,1	0,70	8,54
2000	10	24	5	5	4	1	N	23	TBR	R	10,1	0,87	8,54
2000	11	7	23	4	5	2	S	41	LBT	rLTT	62,6	0,75	7,25
2000	11	9	0	4	4	2	S	71	LBT	rLTT	43,3	0,85	9,90
2000	11	22	1	10	5	2	S	35	RBB	rLTT	48,2	0,76	9,76
2000	11	22	1	4	3	2	S	45	RBB	rLTT	48,2	0,76	9,76
2000	12	12	4	4	3	2	N	29	TBR	LTT	21,6	0,52	9,42
2000	12	13	4	6	2	1	N	40	TBR	LTT	-4,9	0,53	5,82
2000	12	23	1	4	4	1	N	-	TBR	rLTT	7,9	0,58	9,37
2000	12	23	2	3	5	1	N	-	TBR	rLTT	7,5	0,57	9,32
2000	12	24	3	4	4	1	N	-	TBR	LTT	4,4	0,52	8,55
2000	12	25	4	4	4	2	N	22	TBR	LTT	-57,4	0,60	5,49
2001	1	11	4	5	3	0	S	-	TBR	rLTT	38,9	0,76	10,32
2001	5	13	6	7	4	2	S	19	D	TBR	30,6	0,56	10,54
2001	5	25	3	10	5	2	S	31	D	TBR	37,8	0,47	11,47
2001	6	2	0	4	3	1	N	22	D	TBR	30,2	0,77	10,87
2001	7	16	0	4	4	1	S	20	D	TBR	30,9	0,51	10,72
2001	8	12	21	3	3	1	S	-	D	TBR	35,4	0,31	8,52
2001	8	15	23	5	2	0	O	17	D	TBR	33,0	0,70	6,96
2001	8	18	5	5	5	0	S	33	D	TBR	25,5	0,54	9,19
2001	9	2	1	5	3	1	S	17	D	TBR	-28,0	0,73	9,98
2001	9	28	0	12	5	2	S	21	D	LBT	47,4	1,07	9,31

e event start				duration	nr.	class	orient-	λ	bar states		pre-event wave conditions: 24h-averages		
year	*month*	*day*	*hour*	*days*			ation	*m*	*outer*	*inner*	θ [°]	*Hrms [m]*	*Tpeak [s]*
2001	9	28	0	6	5	2	S	-	D	LBT	47,4	1,07	9,31
2001	9	28	0	10	5	1	S	-	D	LBT	47,4	1,07	9,31
2001	9	29	0	5	5	1	S	-	D	RBB	42,0	0,85	8,83
2001	9	29	0	9	2	0	S	-	D	RBB	42,0	0,85	8,83
2002	1	7	23	3	2	0	N	25	TBR	R	-4,7	0,55	9,35
2002	1	18	4	4	2	0	S	23	TBR	R	39,7	0,59	7,15
2002	1	18	4	5	3	1	S	20	TBR	R	39,7	0,59	7,15
2002	1	19	4	5	3	1	S	-	TBR	R	46,7	0,62	5,78
2002	5	14	3	8	3	1	S	22	TBR	rLTT	39,0	0,72	9,65
2002	5	27	3	12	3	2	S	32	TBR	rLTT	41,8	0,78	8,05
2002	5	27	3	3	2	0	S	62	TBR	rLTT	41,8	0,78	8,05
2002	6	6	23	6	3	1	N	32	LBT	LTT	-10,7	0,98	8,31
2002	7	27	4	10	3	2	S	34	LBT	LTT	38,5	0,76	11,19
2002	9	12	21	6	3	1	S	39	TBR	rLTT	44,7	0,89	8,46
2002	10	6	2	14	4	2	N	23	TBR	rLTT	-22,6	0,62	7,40
2002	10	16	23	5	4	2	N	31	TBR	rLTT	14,9	0,43	9,47
2002	10	16	23	10	4	2	N	38	TBR	rLTT	14,9	0,43	9,47
2002	10	23	3	4	4	2	N	36	TBR	rLTT	11,4	0,68	6,50
2002	11	24	5	5	8	2	N	34	TBR	rLTT	3,4	0,49	7,07
2002	11	23	5	8	9	2	N	50	TBR	rLTT	14,4	0,51	7,08
2002	12	11	21	5	12	2	S	44	TBR	rLTT	39,5	0,58	12,02
2003	1	2	2	6	7	2	S	39	eTBR	rLTT	13,9	1,23	11,19
2003	1	26	22	4	6	2	S	31	RBB	rLTT	-1,4	0,66	7,71
2003	1	27	23	3	5	2	S	26	RBB	rLTT	-8,0	0,56	7,83
2003	3	26	23	5	14	2	S	45	RBB	rLTT	36,6	0,63	9,31
2003	3	27	1	6	21	2	S	30	RBB	rLTT	37,7	0,62	9,35
2003	5	8	22	7	3	0	S	23	LBT	RBB	20,3	0,96	9,63
2003	8	12	1	6	4	1	S	40	TBR	rLTT	35,5	0,67	11,31
2003	8	12	1	3	4	2	S	32	TBR	rLTT	35,5	0,67	11,31
2003	8	12	1	3	4	1	S	-	TBR	rLTT	35,5	0,67	11,31
2003	8	25	0	6	11	2	S	33	TBR	rLTT	-22,9	0,54	9,77
2003	8	26	1	4	10	2	S	36	TBR	rLTT	25,1	0,60	12,15
2003	9	8	0	10	3	1	S	35	LBT	rLTT	49,8	0,65	9,42
2003	10	23	0	4	6	2	S	34	RBB	R	-1,0	0,62	9,75

B. Model input parameters (default)

PARAMETERS FOR MORFO62 The following list of parameters and is used in the default setup of MORFO62 for the modelling of the Gold Coast transverse finger bars.

$grav = 9.81$	Gravity acceleration
Discretization	
$NX = 400$	number of collocation points
$OL = 40$	ol*hsca half-points position
$OA = 0.1$	stretching parameter
$OS = 0.95$	stretching parameter for rational Chebyshev
Numerical integration	
$DXNI = 0.1$	x-step for numerical integration
$TOLER1 = 0.050$	water depth at the 'numerical shoreline'
$TOLER2 = 0.0$	water depth at the 'numerical shoreline'
$TOLKD = 0.001$	value of kD below which shallow water approx. is taken
$XMAXNI = 1050$	maximum value of cross-shore coordinate
Numerical parameters	
$VISCO0 = 0.0001$	constant artificial viscosity added for numerical stability
$XMESS = 500.0d0$	offshore cross-shore location at which the sed.transport is set to zero
$DWK = 14.0d0$	offshore water depth where the wind stresses and tidal induced free surface slope decay
$FACDOPPLER = 1.0d0$	factor decreasing the Doppler shift (1=real shift; 0=no shift)
$FACROLLER = 1.0d0$	factor in front of roller radiation stresses on the momnetum equation (1=full terms; 0=
$FACROLLER2 = 0.0d0$	facroller in LSA
$FACWIND = 1.0d0$	factor in front of wind stresses and tidal induced free surface slope on the momentum
$FACSEDSTIR = 0.0d0$	factor in front of the perturbations of the sediment stirring (1=full terms; 0=no pertur
Controles	
$KY1 = 0.11$	initial wave number
$KY2 = 0.35$	final wave number
$KYD = 0.002$	increment of wave number
$SELEJE =' K'$	'0': ky1; 'K': ky1-kyd-¿ky2
$SELMOD = 1$	0:all modes; 1¿selmod¿nteq. selected mode
$DYPLOT = 1.0$	grid increment in 'y'
$XPLOT = 150.00$	max vel in 'x'

Wave Conditions:	
$T_{waves} = 7.5$	wave period
$THETA_{infinity} = 30.0$	wave angle with the shore normal far-offshore
$HRMS_{infinity} = 0.8$	wave height far-offshore
Wind pressure (not used)	
$TAU_x = 0.0d0$	wind shear stresses in the x direction
$TAU_y = 0.0d0$	wind shear stresses in the y direction
$S_y = 0.0d0$	alongshore slope in the free surface elevation
Seafloor and Sediment parameters:	
$BETA_0 = 0.035$	slope at the shoreline for the exponential bottom profile
$D_{infinity} = 18$	water depth far-offshore
$D50 = 2.5E-4$	median grain size
$K_{vis} = 1.36E-6$	kinematic viscosity of water
$POROS = 0.4$	porosity
$S_{rds} = 2.65$	relative density of sediment
$GAMMA = 0.5$	bedslope coefficient
$C_{di} = 2.0E-3$	depth-integrated sediment concentration for the constant stirring case
$EPSI_B = 0.05$	efficiency for resuspension by bores in the Roelvink formulation
$N_{Bor} = 50.0$	n-parameter in the U_{bor} formulation
$M_{Bor} = 1.00$	m- parameter in the U_{bor} formulation and in the Roelvink formulation
SELSTIR = 'B'	
SELDRAG = 'M'	
SELDIFF = 'F'	
	Selstir options:
$'S$	: standard Soulsby van Rijn sediment stirring
$'C'$	constant sediment stirring (c_{da})
$'B'$	bore influence as Renniers inside Soulsby van Rijn stirring
$'R'$	bore stirring as Roelvink added to Soulsby van Rijn stirring
$'K'$	only the bore stirring as Roelvink (alone)
	Seldrag options:
$'C'$	drag coefficient constant = c_d(default)
$'R'$	drag coefficient depth/roughness dependent
$'M'$	drag coefficient of Manning-Strickler law (k_a)
	Seldiff options:
$'U'$	bed-slope coefficient based on Urms (default)
$'V'$	bed-slope coefficient based on V0
$'F'$	bed-slope coefficient based on F_{svr}

Dissipation parameters	
$BW3 = 1.0d0$	coefficient of wave dissipation**3
$G_{wb} = 0.475$	breaking index
$M_{visco} = 1.0$	M-factor of the lateral momentum mixing
$C_D = 0.005$	drag coefficient for bottom friction
$K_a = 0.035$	apparent bed roughness
$Z_{rl} = 1.0E-2$	bed roughness length
$N_{monochr} = 10.0$	n- parameter monochromatic wave parameterization
$M_{monochr} = 10.0$	m-parameter monochromatic wave parameterization
$A_{rol} = 1.0d0$	α factor of wave dissipation on roller enegy
$B_{rol} = 0.05d0$	sin(slope wave front) (where the roller rols)
$SELVISC =' R'$	
$SELFRIC =' MF'$	
$SELDISS =' T'$	
	Selvisc options:
$'C'$	$\nu_t = visco0$
$'R'$	$\nu_t = visco0 + MD(Disipa_{roller}/\rho)^{1/3}$
$'D'$	$\nu_t = visco0 + MD(Disipa/\rho)^{1/3}$
$'L'$	$\nu_t = visco0 + Msqrt(gd)x$ (Longuet Higgins)
$'H'$	$\nu_t = visco0 + MH_{rms}(Disipa/\rho)^{1/3}$ (default)
	Selfric options:
$'C'$	friction coefficient constant = c_d (default)
$'R'$	friction coefficient depth roughness dependent $\rightarrow z_r$
$'M'$	friction coefficient of Manning-Strickler law $\rightarrow k_{[}a]$
$'Q'$	friction term quadratic (default)
$'L'$	friction term linear
$'F'$	Feddersen
$'A'$	friction term from Albert
	Seldiss options:
$'T'$	Thornton-Guza (default)
$'C'$	Church-Thornton
$'M'$	Monochromatic

C. Modification of the model code

In the first series of model runs the rollers were still turned on in both the basic state determination as in the linear stability analysis. This gave very unsatisfying results. Step by step it was tried to improve the result, which proved impossible under the old model setup. To illustrate this there is figure 1, showing the growth rate and migration rate curves, that result a run with the old model setup, in which the parameter 'Facroll' had the value 1.0 in the complete model. When this factor was turned on in the basic state determination but turned off in the LSA, finally smooth and logical growth rate plots resulted, so that it was decided to use this setting in the rest of the analysis. The model code has therefore been changed, defining a 'Facroll1' for the basic state determination, and a ' Facroll2' to use in the linear stability analysis

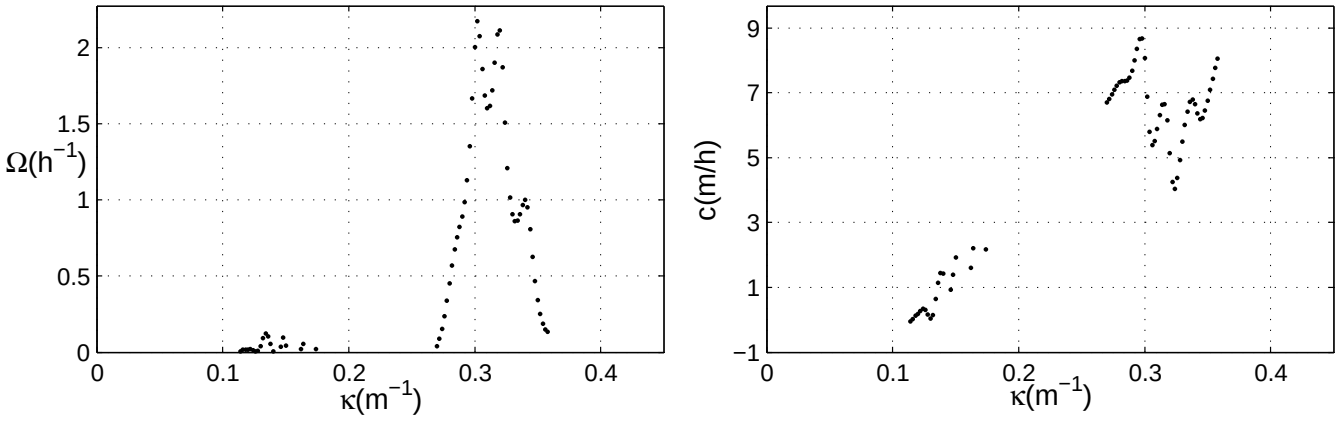

Figure 1: Growth rate curve (left) and migration rate (right) for the default model setup, without defining 'Facroll2 = 0.0' in the LSA-run; here Facroll1 = Facroll2 = 1.0, implying that rollers are taken into account in the complete model.This first mode shows a vague $\omega_{max} = 0.2.17h^{-1}$ for $\kappa = 0.302$, with $c = 6.87m^{h-1}$ here.